Excitonic and nonlinear-optical properties of dielectric quantum-well structures

Masami Kumagai and Toshihide Takagahara
Nippon Telegraph and Telephone Basic Research Laboratories, 3-9-11 Midoricho, Musashino-shi, Tokyo 180, Japan
(Received 18 April 1989)

Excitonic and nonlinear-optical properties of dielectric quantum-well (DQW) structures are investigated theoretically. A DQW is a quantum well sandwiched by barrier materials with a smaller dielectric constant and a larger band gap than the well material. The fundamental physics determining the excitonic properties in a DQW, i.e., exciton binding energy, exciton oscillator strength, and nonlinear-optical response, are clarified. The most important mechanisms for enhancing the excitonic properties are quantum-confinement effect, mass-confinement effect, and dielectric-confinement effect. Quantum confinement increases the spatial overlap between an electron and a hole as a result of the potential well confinement, and it enhances oscillator strength. Mass confinement is based on the penetration of the carrier wave function into barrier layers with a heavier effective mass than the well layer. It increases the exciton reduced mass and hence the exciton binding energy. Dielectric confinement arises from the reduction of the effective dielectric constant of the whole system due to the penetration of the electric field into the barrier medium having a smaller dielectric constant than the well and enhances the Coulomb interaction between the electron and hole. On the basis of these analyses, the general guiding principles are established for designing DQW structures with optimum excitonic properties. Various practical examples of DQW's are examined with respect to the lattice-constant matching, the difference in the dielectric constant, and the difference in the carrier effective masses. ZnSe is found to be one of the most promising candidates for the barrier material of the GaAs DQW.

I. INTRODUCTION

Excitons in semiconductor quantum-well (QW) structures have very sharp peaks in both absorption and luminescence spectra. Their optical and electrical properties are very favorable for optical device application, and many devices using excitonic transitions have been proposed.[1-3] II-VI semiconductors are one of the most appropriate types of material for excitonic transitions because they have a large exciton binding energy and the excitonic transition can be observed clearly. On the other hand, III-V semiconductors generally have small exciton binding energy and show a very broad exciton peak at room temperature.

In the quantum-well structure, the exciton binding energy is greatly enhanced and the optical and electrical properties appear very pronounced.[4] However, even in the limit of two-dimensional confinement, the excitonic binding energy is enhanced at most up to four times the bulk value.[5] Thus in the GaAs quantum-well structure, the exciton binding energy cannot, in principle, be enhanced up to room-temperature energy. The central issue of this paper is how the excitonic binding energy can be enhanced more than that of conventional $GaAs/Al_xGa_{1-x}As$ QW's.

The exciton binding energy in the bulk semiconductor is given by

$$E_{\text{bind}}(\text{bulk})=\frac{e^2}{2\epsilon a_B^*}=\frac{\mu e^4}{2\epsilon^2\hbar^2}\ , \tag{1.1}$$

where a_B^* is the exciton Bohr radius, ϵ is the dielectric constant, and μ is the exciton reduced mass. From this equation, the exciton binding energy is expected to be enhanced by reducing the dielectric constant, or increasing the excitonic reduced mass (i.e., effective masses of the carriers). In addition, confining the carriers in the quantum wells should also enhance the exciton binding energy. The enhancement of the Coulomb interaction in a thin semiconductor layer sandwiched by insulators was pointed out for the first time by Keldysh.[6,7] This effect is caused by the effective reduction of the dielectric constant due to the penetration of electric field into the barrier medium with a small dielectric constant and is called the dielectric confinement effect by analogy to the quantum confinement effect. Recently, we considered a quantum well sandwiched by barrier layers with smaller dielectric constant than the well and called it a dielectric quantum well (DQW).[8,9] In the DQW structure, the dielectric confinement effect reduces the effective dielectric constant of the whole system and also the screening of the electron-hole Coulomb interaction, and hence enhances the exciton binding energy and the excitonic oscillator strength. We discussed the enhancement of the exciton binding energy and of the excitonic optical nonlinearity using the infinite potential barrier model. Although this model is appropriate for a semiconductor-insulator interface, the effect of finite band discontinuities cannot be ignored in general for practical combinations of semiconductors for DQW's. When the band discontinuities are finite, the carrier wave functions extend into the barrier layers and the reduction in the effective dielectric constant of the whole system is more emphasized. At the same time, a completely new effect emerges on the

enhancement of the exciton binding energy. We shall call this effect the mass confinement effect. The carriers feel the heavier masses in the barrier layers through the penetrating part of the wave function and this increases the exciton reduced mass and enhances exciton binding energy. The potential-well (quantum) confinement and the dielectric confinement features in DQW's are shown schematically in Fig. 1. In many cases, the wave function is well confined in the potential well, whereas the static electric field induced by a charge is rather extended due to the long-range character of the Coulomb force. The mass confinement effect depends directly on the potential-well confinement, and has a short-range nature. Thus, the mass confinement effect and the dielectric confinement effect have rather different dependences on the well thickness.

This paper calculates the excitonic states in DQW's using the variational method and taking into account the finite barrier height. The effects of quantum confinement, mass confinement, and dielectric confinement on the excitonic and nonlinear-optical properties in DQW's are clarified for the general case. As a consequence, the guiding principles for designing the DQW structures with optimum excitonic properties are established.

The paper is organized as follows. In Sec. II, the method of calculation of the excitonic state in a DQW structure is presented. In Sec. III, the general features of the exciton in DQW's are discussed, focusing on quantum confinement, dielectric confinement, and mass confinement effects. In Sec. IV, the third-order optical nonlinearity of the DQW structure is investigated on the basis of a general theory of optical nonlinearity in a three-level system. In Sec. V, some practical examples of DQW's are examined, and GaAs/ZnSe and $GaAs/ZnS_xSe_{1-x}$ DQW's are found to be very promising materials for optical devices using the excitonic transition. Section VI is devoted to a summary of the results and conclusions.

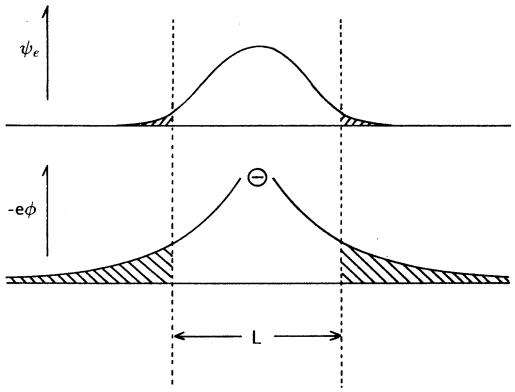

FIG. 1. Confinement features of the one-particle wave function ψ_e and the electrostatic potential ϕ in the quantum-well structure. The hatched portions represent the penetrating wave function and electrostatic potential.

II. METHOD OF CALCULATION

In this section, the method of calculation of the excitonic state in a DQW structure is formulated and a formula for its oscillator strength is derived. A schematic structure of the DQW is shown in Fig. 2. The structure consists of a single quantum well sandwiched by barrier layers having a smaller dielectric constant than the well in order to reduce the effective dielectric constant of the whole system. Throughout this work, only type-I quantum wells are considered because they can have a large exciton binding energy. Finite barrier cases are treated in order to clarify the effect of the effective-mass difference on the excitonic properties, as well as to make the theory more realistic.

The excitonic state in DQW structures should be obtained as an eigenstate of the electron-hole two-particle Hamiltonian. Hamiltonians for the electron, hole, and the electron-hole (exciton) system are given, respectively, as

$$H^{(e)}=H^{(e)}_{\rm kin}+H^{(e)}_{\rm pot}+H^{(e)}_{\rm self}\ , \tag{2.1}$$

$$H^{(h)}=H^{(h)}_{\rm kin}+H^{(h)}_{\rm pot}+H^{(h)}_{\rm self}\ , \tag{2.2}$$

$$H_{\rm tot}=H^{(e)}+H^{(h)}+H_{\rm Coulomb}\ , \tag{2.3}$$

with

$$H^{(e)}_{\rm kin}=\begin{cases}(-\hbar^2/2m_e^{(1)})\nabla_e^2, & |z_e|\le L/2\\ (-\hbar^2/2m_e^{(2)})\nabla_e^2, & |z_e|>L/2\ ,\end{cases} \tag{2.4}$$

$$H^{(h)}_{\rm kin}=\begin{cases}(-\hbar^2/2m_h^{(1)})\nabla_h^2, & |z_h|\le L/2\\ (-\hbar^2/2m_h^{(2)})\nabla_h^2, & |z_h|>L/2\ ,\end{cases} \tag{2.5}$$

$$H^{(e)}_{\rm pot}=\begin{cases}0, & |z_e|\le L/2\\ \Delta E_c, & |z_e|>L/2\ ,\end{cases} \tag{2.6}$$

$$H^{(h)}_{\rm pot}=\begin{cases}0, & |z_h|\le L/2\\ \Delta E_v, & |z_h|>L/2\ .\end{cases} \tag{2.7}$$

Here the suffixes e and h refer to the electron and hole, and the suffixes 1 and 2 stand for the well and the barrier

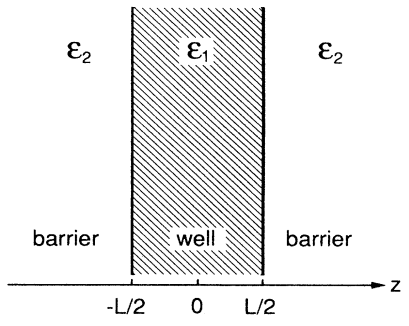

FIG. 2. Schematic diagram of the dielectric quantum-well structure with a smaller dielectric constant in the barrier layer than in the well layer ($\epsilon_2<\epsilon_1$).

layers, respectively. The effect of the dielectric-constant difference between the well and barrier layers is included in the Hamiltonian H_{Coulomb} and H_{self} by introducing image charges. The image-charge method, which is a well-established method in electrostatics, represents the electric field induced by charged particles in the plane-parallel geometries in terms of imaginary charges placed in virtually homogeneous media.

The detailed derivation of H_{Coulomb} and H_{self} is given in Appendix A. Here, the well layer will be denoted by C and the barrier layers by L (left side) and R (right side). The Coulomb interaction between an electron in region A and a hole in region B will be denoted by $H^{AB}_{\text{Coulomb}}(r_e,r_h)$. The explicit expressions of H_{Coulomb} corresponding to five configurations of the electron and hole positions are given as follows:

$$H^{CC}_{\text{Coulomb}}(r_e,r_h)=-\sum_{n=-\infty}^{\infty}\frac{q_n e^2}{\epsilon_1\{(r_{e\parallel}-r_{h\parallel})^2+[z_e-(-1)^n z_h-nL]^2\}^{1/2}}\ , \tag{2.8}$$

$$H^{LC}_{\text{Coulomb}}(r_e,r_h)=-\left[\frac{2\epsilon_1}{\epsilon_1+\epsilon_2}\right]\sum_{n=0}^{\infty}\frac{q_n e^2}{\epsilon_1\{(r_{e\parallel}-r_{h\parallel})^2+[z_e-(-1)^n z_h-nL]^2\}^{1/2}}\ , \tag{2.9}$$

$$H^{RC}_{\text{Coulomb}}(r_e,r_h)=-\left[\frac{2\epsilon_1}{\epsilon_1+\epsilon_2}\right]\sum_{n=0}^{\infty}\frac{q_n e^2}{\epsilon_1\{(r_{e\parallel}-r_{h\parallel})^2+[z_e-(-1)^n z_h+nL]^2\}^{1/2}}\ , \tag{2.10}$$

$$H^{LR}_{\text{Coulomb}}(r_e,r_h)=-\left[\frac{2\epsilon_1}{\epsilon_1+\epsilon_2}\right]^2\sum_{n=0}^{\infty}\frac{q_{2n}e^2}{\epsilon_1[(r_{e\parallel}-r_{h\parallel})^2+(z_e-z_h-2nL)^2]^{1/2}}\ , \tag{2.11}$$

$$H^{RR}_{\text{Coulomb}}(r_e,r_h)=-\left[\frac{2\epsilon_1}{\epsilon_1+\epsilon_2}\right]^2\sum_{n=0}^{\infty}\frac{q_{2n+1}e^2}{\epsilon_1\{(r_{e\parallel}-r_{h\parallel})^2+[z_e+z_h+(2n+1)L]^2\}^{1/2}}$$
$$-\frac{e^2}{\epsilon_2[(r_{e\parallel}-r_{h\parallel})^2+(z_e-z_h)^2]^{1/2}}+\frac{q_1 e^2}{\epsilon_2[(r_{e\parallel}-r_{h\parallel})^2+(z_e+z_h-L)^2]^{1/2}}\ , \tag{2.12}$$

with

$$q_n=\left[\frac{\epsilon_1-\epsilon_2}{\epsilon_1+\epsilon_2}\right]^{|n|}\ . \tag{2.13}$$

The self-energy Hamiltonian has only two forms according to the position of the charged particle. For an electron, they are given as

$$H^{C}_{\text{self}}(r_e)=\frac{q_1 e^2}{2\epsilon_1|2z_e+L+2\delta|}+\frac{q_1 e^2}{2\epsilon_1|2z_e-L-2\delta|}+\sum_{n=\pm2,\pm3,\ldots}\frac{q_n e^2}{2\epsilon_1|z_e-(-1)^n z_e+nL|}\ , \tag{2.14}$$

$$H^{R}_{\text{self}}(r_e)=H^{L}_{\text{self}}(-r_e)=-\frac{q_1 e^2}{2\epsilon_2|2z_e-L+2\delta|}+\left[\frac{2\epsilon_1}{\epsilon_1+\epsilon_2}\right]\sum_{n=0}^{\infty}\frac{q_{2n+1}e^2}{(\epsilon_1+\epsilon_2)|2z_e+(2n+1)L|}\ . \tag{2.15}$$

The self-energy Hamiltonian for a hole is given by simply replacing the suffix e with h in the above expressions. The self-energy potentials diverge at the interface. The divergent terms are separated out of the infinite series of the sums in (2.14) and (2.15). To remedy this divergence, shifted mirror faces[10] are employed for the lowest-order ($n=\pm1$) image charges, introducing the mirror shift δ (Fig. 3). As shown in Fig. 4(a), the self-energy potential has an infinite discontinuity at the interfaces for the original mirror face, while it is suppressed for the shifted mirror face.

First, we will discuss the one-particle wave functions in the DQW structure and then construct the exciton wave function from a product of the one-particle wave functions. It is desirable when calculating the eigenstates of $H^{(e)}$ in (2.1) or $H^{(h)}$ in (2.2) to include the self-energy potential. As shown in Fig. 4(b), the self-energy potential

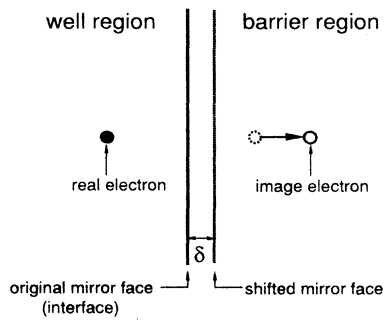

FIG. 3. Shifted mirror face and the image electron. The shifted mirror face is introduced to suppress the divergent feature of the self-Coulomb interaction. Original mirror face is at the interface, and the shifted mirror face is located a distance δ from the interface. The solid line represents the true interface and the dashed line represents the shifted mirror face.

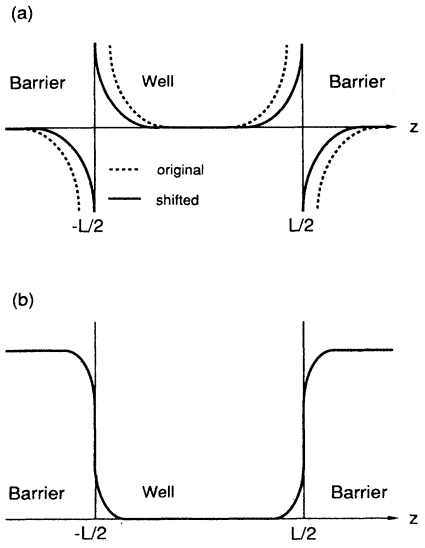

FIG. 4. Qualitative features of (a) the self-energy potential for the original and the shifted interfaces and (b) the effective one-particle potential including the self-energy potential ($H_{\rm pot}+H_{\rm self}$).

changes the square-well potential into a smoothly shaped potential but the confinement feature is not essentially modified. Thus the eigenstates of $H_0^{(e)}=H_{\rm kin}^{(e)}+H_{\rm pot}^{(e)}$ or $H_0^{(h)}=H_{\rm kin}^{(h)}+H_{\rm pot}^{(h)}$ can be employed as a good approximation for the true eigenstates of $H^{(e)}$ or $H^{(h)}$.

The lowest eigenstates of $H_0^{(e)}$ is obtained in the form

$$\psi_e(z_e)=\begin{cases}\cos(k_e z_e), & |z_e|\le L/2\ ,\\ B_e\exp(-\kappa_e|z_e|), & |z_e|>L/2\ ,\end{cases} \tag{2.16}$$

where the parameters k_e, κ_e, and B_e are determined through the conventional treatment of the square-well potential problem. Here, we use the following boundary conditions (see Appendix B):

$$\psi_e\left[\frac{L}{2}-0\right]=\psi_e\left[\frac{L}{2}+0\right]\ , \tag{2.17}$$

$$\frac{1}{m_e^{(1)}}\frac{d}{dz_e}\psi_e\left[\frac{L}{2}-0\right]=\frac{1}{m_e^{(2)}}\frac{d}{dz_e}\psi_e\left[\frac{L}{2}+0\right]\ . \tag{2.18}$$

Then the secular equation which determines the energy eigenvalues is obtained as

$$\Delta E_c-\frac{\hbar^2k_e^2}{2m_e^{(1)}}\left[\left[\frac{m_e^{(2)}}{m_e^{(1)}}\right]\tan^2\left[\frac{k_eL}{2}\right]+1\right]=0\ . \tag{2.19}$$

In the same way, the hole wave function is obtained as

$$\psi_h(z_h)=\begin{cases}\cos(k_h z_h), & |z_h|\le L/2\ ,\\ B_h\exp(-\kappa_h|z_h|), & |z_h|>L/2\ ,\end{cases} \tag{2.20}$$

where the parameters k_h, κ_h, and B_h are determined by (2.17), (2.18), and (2.19) simply by replacing the suffix e by h and changing ΔE_c to ΔE_v.

For the lowest exciton state a variational wave function is constructed from a product of the lowest one-particle wave functions of an electron and a hole as

$$\Psi=A\psi_e(z_e)\psi_h(z_h)g(r_{e\parallel}-r_{h\parallel},z_e-z_h)\ , \tag{2.21}$$

where A is the normalization constant and $g(r_{e\parallel}-r_{h\parallel},z_e-z_h)$ represents the electron-hole relative motion, and is defined as

$$g(r_{e\parallel}-r_{h\parallel},z_e-z_h)=\exp\{-[\alpha^2(r_{e\parallel}-r_{h\parallel})^2+\beta^2(z_e-z_h)^2]^{1/2}\}\ . \tag{2.22}$$

Here, α and β are variational parameters to minimize the exciton energy. They represent the confinement in the directions parallel and perpendicular to the interface, respectively. Then the exciton binding energy is defined by

$$E^{\rm bind}\equiv(E^{(e)}+E^{(h)})-E^{\rm tot}\ , \tag{2.23}$$

where the total energy $E^{\rm tot}$ is determined by minimizing the expectation value of the total Hamiltonian by varying the parameters α and β, i.e.,

$$E^{\rm tot}=\min_{\alpha,\beta}\langle\Psi|H_{\rm tot}|\Psi\rangle\ . \tag{2.24}$$

Details of this calculation are given in Appendix C. The one-particle energies are approximated as

$$E^{(e)}\cong\langle\psi_e|H_0^{(e)}+H_{\rm self}^{(e)}|\psi_e\rangle=E_0^{(e)}+\langle\psi_e|H_{\rm self}^{(e)}|\psi_e\rangle\ , \tag{2.25}$$

$$E^{(h)}\cong\langle\psi_h|H_0^{(h)}+H_{\rm self}^{(h)}|\psi_h\rangle=E_0^{(h)}+\langle\psi_h|H_{\rm self}^{(h)}|\psi_h\rangle\ , \tag{2.26}$$

where $E_0^{(e)}$ and $E_0^{(h)}$ are the lowest eigenvalues of $H_0^{(e)}$ and $H_0^{(h)}$, respectively, and the self-energies are included in the lowest-order perturbation theory. Thus the exciton binding energy is calculated approximately by

$$E^{\rm bind}\cong E^b\equiv E_0^{(e)}+E_0^{(h)}+\langle\psi_e|H_{\rm self}^{(e)}|\psi_e\rangle+\langle\psi_h|H_{\rm self}^{(h)}|\psi_h\rangle-E^{\rm tot}\ . \tag{2.27}$$

The mirror shift δ is introduced phenomenologically because the first-principles determination of δ is beyond the scope of this paper. At present there is no criterion for appropriate choice of the value of δ. However, fortunately enough, we find that physical quantities, such as the exciton binding energy, are not very strongly dependent on the parameters δ. The calculated δ dependence of the exciton binding energy is shown in Fig. 5. The well and barrier materials are chosen to be GaAs and ZnSe, respectively, in order to see the δ dependence of the exciton binding energy under realistic situations. The material parameters used in this calculation are given in Table V. The exciton binding energy is measured in units of the effective Rydberg of GaAs and the well width is measured in units of the exciton Bohr radius in GaAs. The effective Rydberg and the exciton Bohr radius of GaAs are estimated as 5 meV and 114 Å, respectively, by using the static dielectric constant and the carrier masses of bulk GaAs given in Table V. It can be seen from the

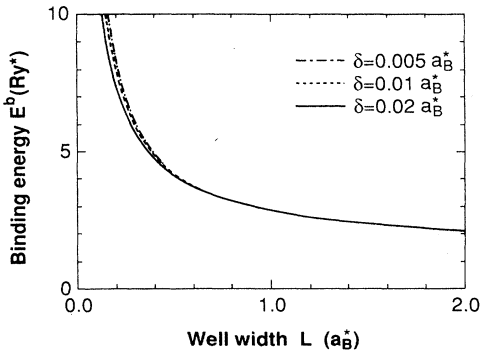

FIG. 5. Mirror shift δ dependence of the exciton binding energy. Three δ values are employed. The binding energy and the well width are scaled by the effective Rydberg (Ry*), namely the exciton binding energy and by the exciton Bohr radius (a_B^*) of the bulk well material, respectively.

figure that the δ dependence of the exciton binding energy is rather weak, except for the very thin layer case. The difference in the exciton binding energy between the two cases $\delta/a_B^*=0.01$ and 0.02 are 1.1% and 5.3% for the well width $L=0.5$ and $0.2a_B^*$, respectively. Thus the exciton binding energy and also the exciton oscillator strength can be calculated precisely enough so far as the mirror shift δ is chosen appropriately.

The oscillator strength of the excitonic transition is calculated in order to clarify the optical properties of the excitons in DQW's. The oscillator strength of the excitonic transition is defined by[11]

$$f_{e,\mathbf{K}}=\frac{2}{m_0\hbar\omega_{eg,\mathbf{K}}}|\langle e,\mathbf{K}|M|g\rangle|^2 . \tag{2.28}$$

Here, $|g\rangle$ stands for the ground state, m_0 is the free electron mass, $\omega_{eg,\mathbf{K}}$ the angular frequency of the excitonic transition, and M is given by

$$M=\frac{\mathbf{p}\cdot e^{i\mathbf{K}\cdot\mathbf{r}}+e^{i\mathbf{K}\cdot\mathbf{r}}\cdot\mathbf{p}}{2} , \tag{2.29}$$

in terms of the momentum operator $\mathbf{p}$. The exciton state $|e,\mathbf{K}\rangle$ with a total wave vector $\mathbf{K}$ can be written as

$$|e,\mathbf{K}\rangle=\left[\frac{\sigma_0}{N_\parallel}\right]^{1/2} d_0\sum_{\mathbf{r}_e,\mathbf{r}_h} e^{i\mathbf{K}\cdot\mathbf{R}_\parallel}\Psi(\mathbf{r}_{e\parallel}-\mathbf{r}_{h\parallel},z_e,z_h) \times a^\dagger_{c\mathbf{r}_e}a_{v\mathbf{r}_h}|g\rangle , \tag{2.30}$$

where the second-quantized form in the Wannier orbital representation is employed and $\mathbf{R}_\parallel$ denotes the center-of-mass coordinate parallel to the interface, σ_0 and d_0 denote the area and the length of a unit cell in the direction parallel and perpendicular to the interface, and $N_\parallel$ gives the number of unit cells in the quantization area. The oscillator strength is usually defined for the active volume of the quantum well. However, the active volume is not well defined for the quantum-well structure with finite potential barrier because the exciton wave function is extended into the barrier layers. Here, the oscillator strength per unit volume is calculated by dividing the oscillator strength by the effective volume $V=L\sigma_0N_\parallel$:

$$\bar{f}_{e,\mathbf{K}}=\frac{f_{e,\mathbf{K}}}{V}=\frac{2p_{eg}^2}{m_0\hbar\omega_{eg,\mathbf{K}}}\frac{Q^2}{L} , \tag{2.31}$$

with

$$Q=\int\Psi(0,z_e,z_e)dz_e , \tag{2.32}$$

where p_{eg} is the interband momentum matrix element. Substituting (2.21) into (2.32) with (2.16) and (2.20), we obtain

$$Q=A\left[\frac{\sin(k_e-k_h)L/2}{k_e-k_h}+\frac{\sin(k_e+k_h)L/2}{k_e+k_h} +\frac{2B_eB_h}{\kappa_e+\kappa_h}e^{-(\kappa_e+\kappa_h)L/2}\right] . \tag{2.33}$$

To see the enhancement factor explicitly, the oscillator strength is compared to that of the bulk material:

$$\frac{\bar{f}_{e,\mathbf{K}}}{f_{\text{bulk}}}=\frac{\omega_{\text{bulk}}}{\omega_{\text{DQW}}}\frac{\pi a_B^{*3}Q^2}{L} , \tag{2.34}$$

where a_B^* is the exciton Bohr radius in the bulk material and ω_{DQW} and ω_{bulk} denote the excitonic transition frequencies in the DQW and in the bulk material, respectively. The first factor is related to the energy shift due to the quantum confinement and this quantity cannot be determined without specifying the band-gap energy of the DQW material. However, to see the general trends of the oscillator strength, it is not necessary to specify the band-gap energy. Thus the oscillator-strength ratio is calculated dropping the frequency factor as

$$\tilde{f}\equiv\frac{\pi a_B^{*3}Q^2}{L}\simeq\frac{\bar{f}_{e,\mathbf{K}}}{f_{\text{bulk}}} . \tag{2.35}$$

The dependence of this quantity on the potential barrier height, the dielectric-constant ratio, and the effective-mass ratio will be discussed in Sec. III.

III. GENERAL FEATURES OF DQW's

The optimum design of a synthesized material requires precise knowledge of the fundamental properties and their dependence on physical parameters of the original materials as well as on details of the structure. In this section, the general properties of the excitons in DQW's

TABLE I. Parameters of the model well material. All DQW's appearing in Sec. III have this well material. The electron and hole effective masses m_e and m_h are measured in units of the free electron mass m_0.

Sample	Well material
$m_e^{(1)}$ (m_0)	0.1
$m_h^{(1)}$ (m_0)	0.5
ϵ_1	10

TABLE II. Parameters of the model barrier materials in No. 1-1, No. 1-2, No. 1-3, and No. 1-4. The conduction- (valence-) band discontinuity ΔE_c (ΔE_v) is measured in units of the effective Rydberg of the well material.

Sample	No. 1-1	No. 1-2	No. 1-3	No. 1-4
ΔE_c (Ry*)	10	10	100	100
ΔE_v (Ry*)	10	100	10	100
$m_e^{(2)}$ (m_0)	0.1	0.1	0.01	0.1
$m_h^{(2)}$ (m_0)	0.5	0.5	0.5	0.5
ϵ_2	5	5	5	5

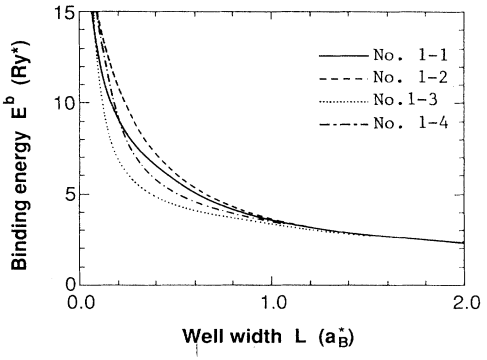

FIG. 6. Calculated exciton binding energy of the four model DQW's No. 1-1, No. 1-2, No. 1-3, and No. 1-4, which have the same well material and whose barrier materials have the same parameters except for the band discontinuity. The material parameters of the well and barrier layers are given in Tables I and II, respectively. The binding energy is scaled by the effective Rydberg (Ry*), namely the exciton binding energy and the well width is scaled by the exciton Bohr radius (a_B^*) of the bulk well material

are clarified by using model materials. The main subjects are the effects of barrier height of the DQW, effective mass of the electron and hole in the barrier layer, and dielectric constant of the barrier layer. The material parameters of the well layer are given in Table I, and the parameters are chosen similar to those of GaAs to simulate a realistic situation. This well material is used throughout this section.

A. Effect of the barrier height

First, the barrier-height dependence of the exciton binding energy is investigated. To examine this dependence, four barrier materials having different barrier heights are considered. Table II gives the material parameters of these barrier materials. They have the same values of the electron and hole masses and of the dielectric constant except for the band discontinuity. The band discontinuities are measured in the effective Rydberg (Ry*), namely the bulk excitonic binding energy of the well material.

Figure 6 shows the exciton binding energy E^b in the four DQW's as a function of the well width. The well width is normalized by the excitonic Bohr radius in the bulk well material and the exciton binding energy is measured in units of the effective Rydberg. The binding energy increases by reducing the well width for all four cases. For thick layers ($L \gtrsim 1.6a_B^*$), the four DQW's have almost an identical exciton binding energy, and the larger band discontinuity (stronger confinement) yields the larger binding energy. These trends are the same as those in the conventional quantum wells (QW's) where the dielectric confinement effect can be neglected. On the other hand, for thin layers, the situation becomes very complex and the sample with the largest band discontinuities for both conduction and valence bands (No. 1-4) does not have the largest binding energy. In order to see the origin of the complicated behavior, we rewrite the exciton binding energy as

$$
\begin{aligned}
E^b &\equiv \langle \psi_e | H^{(e)} | \psi_e \rangle + \langle \psi_h | H^{(h)} | \psi_h \rangle - \langle \Psi_{\min} | H_{\rm tot} | \Psi_{\min} \rangle \ , \\
&= (\langle \psi_e | H^{(e)}_{\rm kin} + H^{(e)}_{\rm pot} | \psi_e \rangle + \langle \psi_h | H^{(h)}_{\rm kin} + H^{(h)}_{\rm pot} | \psi_h \rangle - \langle \Psi_{\min} | H^{(e)}_{\rm kin} + H^{(h)}_{\rm kin} + H^{(e)}_{\rm pot} + H^{(h)}_{\rm pot} + H_{\rm Coulomb} | \Psi_{\min} \rangle) \\
&\quad + (\langle \psi_e | H^{(e)}_{\rm self} | \psi_e \rangle + \langle \psi_h | H^{(h)}_{\rm self} | \psi_h \rangle - \langle \Psi_{\min} | H^{(e)}_{\rm self} + H^{(h)}_{\rm self} | \Psi_{\min} \rangle) \ , \qquad (3.1)
\end{aligned}
$$

where $\Psi_{\min}$ is the variationally determined exciton wave function. The quantity within the first set of parentheses can be regarded approximately as the exciton binding energy in the conventional QW's, although $\Psi_{\min}$ includes the dielectric confinement effect through the variational parameters α and β in (2.22). In fact, this quantity takes the largest value for No. 1-4, reflecting the strongest quantum confinement. On the other hand, the quantity within the second set of parentheses represents the difference between one-electron self-energy and exciton self-energy. The relative magnitude of the self-energy difference among DQW's of No. 1 series is rather complicated and cannot be interpreted in a simple manner. Thus, although the larger band discontinuities yield larger Coulomb interaction between an electron and a hole, the self-energy difference compensates the enhanced Coulomb interaction, resulting in a rather complex behavior of the exciton binding energy.

The oscillator strength of the excitonic transition for these samples is shown in Fig. 7. Generally, the oscillator strength increases monotonically as the well width is reduced. This results from the increased spatial overlap between the electron and the hole due to the confinement effect. However, the barrier-height dependence of the oscillator strength is rather complex. It can be seen that higher potential barrier yields larger oscillator strength

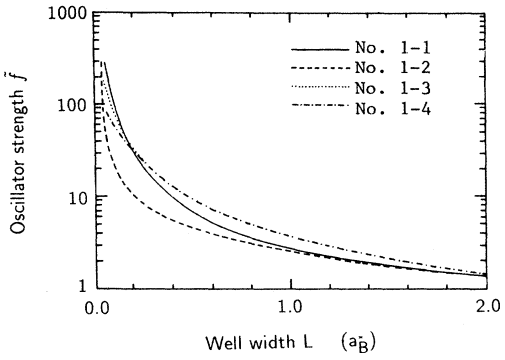

FIG. 7. Calculated exciton oscillator strength of the four model DQW's No. 1-1, No. 1-2, No. 1-3, and No. 1-4 normalized by the value of bulk GaAs. The dotted line (No. 1-3) becomes almost identical to the dot-dashed line (No. 1-4) for $L > 0.2a_B^*$.

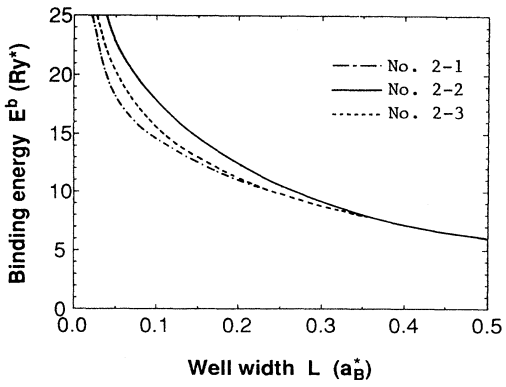

FIG. 8. Calculated exciton binding energy of the three model DQW's No. 2-1, No. 2-2, and No. 2-3 which have the same material parameters except for carrier masses in the barrier layer. The relevant material parameters of the well and barrier layers are given in Table I and III, respectively.

except for the extremely thin region ($L < 0.2a_B^*$). This tendency can be explained as a consequence of the potential barrier confinement. It can be also seen that the increase in the oscillator strength due to the confinement effect is stronger for the electron than for the hole.

B. Effect of the effective mass of the barrier

As mentioned in Sec. I, the effective mass of the carriers in the barrier layer plays an important role in determining the excitonic state. The effect of the effective mass is closely related to the confinement of the wave function, because the wave function penetrates the barrier layer and is affected by the effective mass of the barrier. Table III gives the material parameters of the model barrier materials. They all have the same barrier heights ($\Delta E_c = 10$, $\Delta E_v = 100$) and dielectric constant ($\epsilon_2 = 5$). Barrier material No. 2-1 has the same electron and hole effective masses as the well material. Material No. 2-2 has 5 times the electron effective mass of the well material and the same hole effective mass as the well. On the other hand, material No. 2-3 has five times the hole effective mass of the well material and the same electron effective mass as the well.

Figure 8 shows the exciton binding energy for materials No. 2-1, No. 2-2, and No. 2-3. Material No. 2-2 yields the largest binding energy among these samples. This can be explained in terms of the difference in the exciton reduced mass of the barrier material, which is 1, 3, and 1.15 times that of the well material for No. 2-1, No. 2-2, and No. 2-3, respectively. Thus the exciton binding energy in No. 2-2 is enhanced through the penetration of the exciton wave function into the barrier layer.

The oscillator strength of the excitonic transition is also calculated for these DQW's and the results are shown in Fig. 9. General trends of these curves are similar to those of the exciton binding energy. For thin layers ($L < 0.8a_B^*$), material No.2-2 has the largest oscillator strength corresponding to the largest binding energy. This is a consequence of decrease in the exciton Bohr radius due to the mass confinement effect. For thick layers, the difference among three materials is small.

Summarizing the barrier-mass effect, the barrier material should have a large carrier mass to enhance excitonic properties. The barrier-mass effect is more pro-

TABLE III. Parameters of the model barrier materials in No. 2-1, No. 2-2, and No. 2-3. Notations are the same as in Table II.

Sample	No. 2-1	No. 2-2	No. 2-3
ΔE_c (Ry*)	10	10	10
ΔE_v (Ry*)	100	100	100
$m_e^{(2)}$ (m_0)	0.1	0.5	0.1
$m_h^{(2)}$ (m_0)	0.5	0.5	2.5
ϵ_2	5	5	5

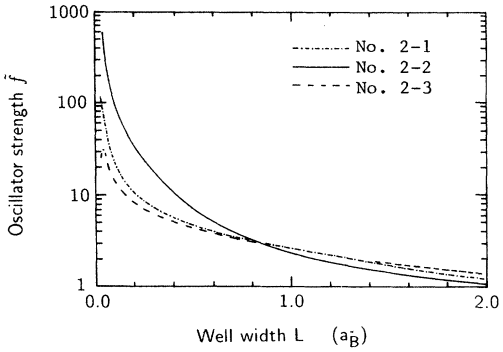

FIG. 9. Calculated exciton oscillator strength of the three model DQW's No. 2-1, No. 2-2, and No. 2-3 normalized by the value of bulk GaAs.

nounced for a lighter mass carrier (electrons for many cases) than for a heavier mass carrier since the exciton reduced mass is determined mainly by the lighter carrier mass.

C. Effect of the dielectric constant of the barrier

The effect of the difference in dielectric constant between the well and barrier layers was the initial motive for investigating DQW structures. We have already studied this effect using the infinite barrier model.[8,9] However, the infinite barrier model is not appropriate for very thin well layers because the unphysically localized wave function yields an extremely large Coulomb interaction between the electron and the hole, and consequently the calculated results are not reliable. To see the effect of the dielectric-constant difference in a more realistic situation, we examined four model barrier materials No. 3-1, No. 3-2, No. 3-3, and No. 3-4 which have the same material parameters except for the dielectric constant ($\epsilon_2 = 10, 5, 2$, and 1). Their material parameters are given in Table IV.

The exciton binding energies of these materials are shown in Fig. 10. The exciton binding energy can be enhanced by decreasing the dielectric constant of the barrier. This enhancement clearly lasts up to the region of $L \gtrsim 2a_B^*$, while the effect of barrier mass disappears around the region of $L \gtrsim a_B^*$ as was seen in Sec. III B. This is a direct consequence of the long-range nature of the polarization effect. The most important features is that the extremely large binding energy exceeding the two-dimensional limit (4 Ry*) can be obtained by decreasing the barrier dielectric constant. This large enhancement can produce a very stable exciton even when the well material originally had a small binding energy.

The oscillator strength of the excitonic transition is also calculated, and the results are shown in Fig. 11. The oscillator strength becomes larger as the barrier dielectric constant is reduced. This is due to the reduction in the effective electron-hole distance through the dielectric confinement effect.

In order to see these general features in a practical DQW, the exciton binding energy in GaAs/ZnSe DQW's is plotted in Fig. 12 as a function of the well width. Four curves are shown in the figure: the solid line corresponds to the GaAs/ZnSe DQW's, the dot-dashed line to a hypothetical DQW in which ZnSe is assumed to have the same carrier masses as GaAs, the dashed line to another hypothetical DQW in which ZnSe is assumed to have the same dielectric constant as GaAs, and the dotted line to a hypothetical DQW in which ZnSe is assumed to have the same dielectric constant and carrier masses as GaAs. In these hypothetical DQW's, the band discontinuities are taken to be the same as the realistic values. Details of the material parameters used in the calculation is given in Sec. V. It is found that the dielectric confinement effect is dominantly contributing to the enhancement of the exciton binding energy in this system. It is also confirmed that the carrier mass effect is effective only for thin well layers, whereas the dielectric effect works even for thicker layers.

In summary, DQW structures have excitonic properties which can be readily controlled by changing the barrier material. We have three degrees of freedom in controlling the excitonic properties in DQW's. One is the barrier height, which determines the one-particle confinement feature; the change in the band discontinuity yields the change in the excitonic properties. Another is the effective mass of carriers in the barrier, which affects the excitonic properties through the change in the exci-

TABLE IV. Parameters of the model barrier materials in No. 3-1, No. 3-2, No. 3-3, and No. 3-4. Notations are the same as in Table II.

Sample	No. 3-1	No. 3-2	No. 3-3	No. 3-4
ΔE_c (Ry*)	10	10	10	10
ΔE_v (Ry*)	100	100	100	100
$m_e^{(2)}$ (m_0)	0.5	0.5	0.5	0.5
$m_h^{(2)}$ (m_0)	0.5	0.5	0.5	0.5
ϵ_2	10	5	2	1

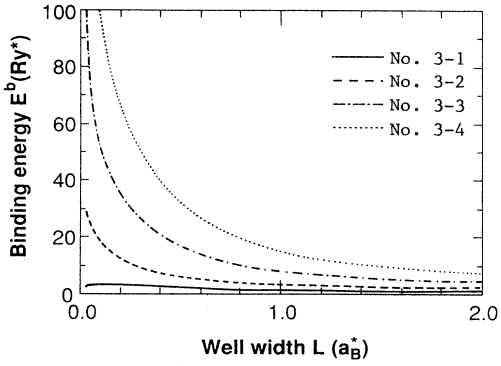

FIG. 10. Calculated exciton binding energy of the four model DQW's No. 3-1, No. 3-2, No. 3-3, and No. 3-4 which have the same material parameters except for the dielectric constant of the barrier layer. The relevant material parameters of the well and barrier layers are given in Tables I and IV, respectively.

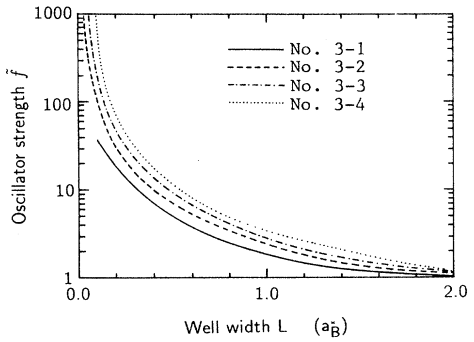

FIG. 11. Calculated exciton oscillator strength of the four model DQW's, No. 3-1, No. 3-2, No. 3-3, and No. 3-4 normalized by the value of bulk GaAs.

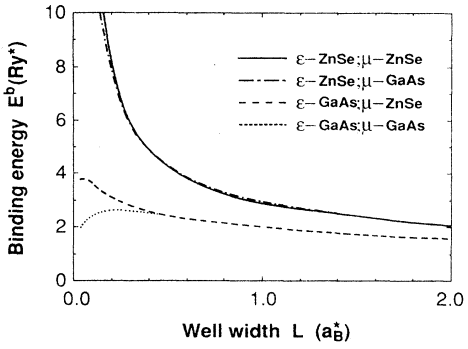

FIG. 12. Exciton binding energy of the GaAs/ZnSe DQW (solid line). In order to clarify the mass confinement and dielectric confinement effects, three virtual barrier materials are considered: one with the dielectric constant of ZnSe and carrier masses of GaAs (dot-dashed line), another with the dielectric constant of GaAs and carrier masses of ZnSe (dashed line), and the other with dielectric constant and carrier masses of GaAs (dotted line). The material parameters used in the calculation are given in Table V.

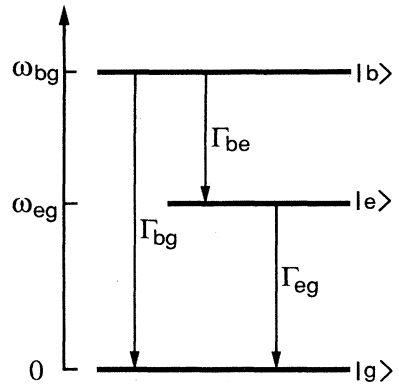

FIG. 13. Energy diagrams of a three-level model. $|g\rangle$, $|e\rangle$, and $|b\rangle$ denote the ground, the one-exciton, and two-exciton states, respectively. Three longitudinal relaxation constants are shown with associated transitions.

ton reduced mass. The change in the mass of the lighter carrier (electron) gives the larger change in the excitonic properties. The other is the dielectric constant of the barrier. This quantity dominates the electrostatic feature of the DQW, and determines the excitonic properties. We can get the optimum enhancement of the excitonic properties by combining these three effects.

IV. OPTICAL NONLINEARITY OF DQW's

In this section, the calculation of the third-order optical nonlinearity of DQW's is presented. This calculation is based on the three-level model given in Fig. 13. The ground, one-exciton, and two-exciton states are denoted by $|g\rangle$, $|e\rangle$, and $|b\rangle$, respectively. Energy separation between $|g\rangle$ and $|e\rangle$ is denoted by $\hbar\omega_{eg}$, and that between $|e\rangle$ and $|b\rangle$ by $\hbar\omega_{be}$. Six relaxation constants are included in the model; three of them representing the longitudinal relaxation rates and the other three representing the transverse relaxation rates. Here, the third-order nonlinear susceptibility $\chi^{(3)}$ is defined by the following relation between the third-order nonlinear polarization $\mathbf{P}^{(3)}$ and the electric field $\mathbf{E}_i$:[12]

$$\mathbf{P}^{(3)}(\omega_1+\omega_2+\omega_3)=\chi^{(3)}(-\omega_1-\omega_2-\omega_3=\omega_1,\omega_2,\omega_3):\mathbf{E}_1(\omega_1)\mathbf{E}_2(\omega_2)\mathbf{E}_3(\omega_3)\ , \tag{4.1}$$

with

$$\mathbf{E}_i(\pm\omega_i)=\mathbf{E}_{0i}\exp(i\mathbf{k}\cdot\mathbf{r}\mp i\omega_i t)\ , \tag{4.2}$$

$$\mathbf{P}^{(3)}(\pm\omega)=\mathbf{P}_0^{(3)}\exp(i\mathbf{k}\cdot\mathbf{r}\mp i\omega t)\ . \tag{4.3}$$

The third-order nonlinear susceptibility is calculated as[13]

$$\begin{aligned}\chi^{(3)}(-\Omega;\Omega,\Omega,-\Omega)=-\frac{e^4}{4\hbar\Omega^3 m_0^2 N_{\parallel}\sigma_0 L}\sum_{e,b}\Bigg[&4\left[\frac{\gamma_{eg}}{\Gamma_{eg}}\right]\omega_{eg}\frac{f_{eg}^2}{(\omega_{eg}-\Omega-i\gamma_{eg})^2(\omega_{eg}-\Omega+i\gamma_{eg})}\\&-2\left[\frac{\gamma_{eg}}{\Gamma_{eg}}\right]\omega_{eg}\frac{f_{eg}f_{be}}{(\omega_{be}-\Omega-i\gamma_{be})(\omega_{eg}-\Omega-i\gamma_{eg})(\omega_{eg}-\Omega+i\gamma_{eg})}\\&-\omega_{be}\frac{f_{eg}f_{be}}{(\omega_{eg}-\Omega-i\gamma_{eg})^2(\omega_{bg}-2\Omega-i\gamma_{gb})}\\&+\omega_{eg}\frac{f_{eg}f_{be}}{(\omega_{be}-\Omega-i\gamma_{be})(\omega_{bg}-2\Omega-i\gamma_{bg})(\omega_{eg}-\Omega-i\gamma_{eg})}\Bigg]\ ,\end{aligned} \tag{4.4}$$

where Ω is the frequency of the incident light, ω_{ij} (f_{ij}) is the frequency (oscillator strength) of transition between i and j states, the notations σ_0 and $N_{\parallel}$ were given in Sec. II, and the summation is taken over the exciton states.

Γ_{ij} is the longitudinal relaxation rate between i and j states, and γ_{ij} is the relaxation rate of the off-diagonal ($i \neq j$) element of the density matrix (transverse relaxation rate). The transverse relaxation rate γ_{ij} is generally composed of the sum of the decay rate of the amplitude of the i and j state wave functions (γ'_{ij}) and the pure dephasing rate (γ''_{ij}):

$$\gamma_{ij} \equiv \gamma'_{ij} + \gamma''_{ij} . \tag{4.5}$$

The oscillator strength given by (2.29) is defined for the free exciton which moves coherently throughout the whole crystal corresponding to a δ-function-like spectrum of the exciton. This oscillator strength is proportional to the quantization volume and becomes infinitely large as the quantization volume increases. Correspondingly, the radiative lifetime of excitons becomes infinitely short and at the same time the $\chi^{(3)}$ value diverges since $\chi^{(3)}$ is proportional to the square of the oscillator strength. This unphysical situation was recently resolved by Feldmann *et al.*[14] by introducing the concept of coherence volume which is determined by the homogeneous linewidth of the exciton transition. In their interpretation, the infinitely large oscillator strength of the $K=0$ exciton is shared by the finite-momentum exciton states within the spectral linewidth Δ. Since the number of states within the spectral linewidth Δ is proportional to the quantization volume, the redistributed oscillator strength for each exciton state becomes finite. This effective oscillator strength successfully explains the dependence of radiative lifetime on the sample temperature and on the quantum-well thickness.[14] Using this interpretation, the intensive character of $\chi^{(3)}$ can be recovered as shown below.

The $K=0$ oscillator strength f_{ij} and the effective oscillator strength F_{ij} in DQW's can be written as

$$f_{ij} = N_{\parallel}\sigma_0 \frac{2Q^2}{m_0 \hbar \omega_{ij}} |p_{ij}|^2 , \tag{4.6}$$

$$F_{ij} = \left[\frac{2\pi\hbar^2}{M\Delta} \right] \frac{2Q^2}{m_0 \hbar \omega_{ij}} |p_{ij}|^2 , \tag{4.7}$$

where p_{ij} is the momentum matrix element between i and j states, M is the translational mass of the exciton parallel to the interface, and Q is given in (2.33). The $K=0$ oscillator strength f_{ij} becomes infinitely large when the quantization area $N_{\parallel}\sigma_0$ is taken to be infinite. On the other hand, the effective oscillator strength is not proportional to the quantization area but to another quantity with the same dimensions. This can be called the coherence area of exciton in a quantum-well structure:

$$S_{\mathrm{coh}} = \frac{2\pi\hbar^2}{M\Delta} . \tag{4.8}$$

Hence the coherence volume of exciton can be given by $S_{\mathrm{coh}}L$. In fact, the oscillator strength F_{ij} is equal to $S_{\mathrm{coh}}L$ times the unit-volume oscillator strength in (2.31).

Now, we define the effective nonlinear susceptibility $\chi^{(3)}$ by summing the nonlinear polarization due to each exciton state distributed over the spectral width Δ as

$$\chi^{(3)} = \int_{\Delta} \hat{\chi}^{(3)}(E) D(E) dE , \tag{4.9}$$

where E stands for the transition energies $\hbar\omega_{eg}$ and $\hbar\omega_{be}$, $\hat{\chi}^{(3)}(E)$ is given by (4.4) replacing the oscillator strength f_{ij} by F_{ij} and dropping the summation symbol, and the density of states $D(E)$ is given as

$$D(E) = \frac{MN_{\parallel}\sigma_0}{2\pi\hbar^2} . \tag{4.10}$$

If the spectral width Δ is so small that the energy dependence of $\hat{\chi}^{(3)}(E)$ can be neglected, we have

$$\chi^{(3)} \cong \frac{N_{\parallel}\sigma_0}{S_{\mathrm{coh}}} \hat{\chi}^{(3)}(E) . \tag{4.11}$$

Now it is easy to check the intensive character of $\chi^{(3)}$. In the above calculation we ignored the temperature factor defined by

$$\zeta(T) = \frac{\int_{\Delta} D(E) f(E) dE}{\int_0^{\infty} D(E) f(E) dE} , \tag{4.12}$$

where f is the Bose distribution function. This factor must be taken into account to see the effect of finite temperature on $\chi^{(3)}$. Here, we scale $|p_{be}|^2$ as

$$|p_{be}|^2 = \xi |p_{eg}|^2 . \tag{4.13}$$

In the bulk crystal, ξ is estimated to be 1/2 for a weakly bound biexciton state composed of spin-singlet pairs of electrons and holes, whereas for two-exciton scattering (unbound) state, ξ is estimated to be 2 corresponding to the boson model.[13] In low-dimensional structures, ξ takes a value between these two values depending on the details of the envelope wave function. We also assume that

$$\Gamma_{bg} = 0 . \tag{4.14}$$

This assumption implies that the two-exciton state cannot be annihilated radiatively by single photon emission apart from two-photon cascade emission via the one-exciton state. Then $\chi^{(3)}$ can be written as

$$\chi^{(3)} = \frac{\omega_{eg} e^4}{2m_0^2 \Omega^3 \hbar \Gamma_{eg} \gamma_{eg}^2} \frac{S_{\mathrm{coh}}}{L_z} \left[\frac{2Q^2}{m_0 \hbar \omega_{eg}} |p_{eg}|^2 \right]^2 h_0(\Omega) , \tag{4.15}$$

and the dimensionless frequency factor $h_0(\Omega)$ is given by

$$h_0(\Omega)=-\frac{2(\omega_{be}-\Omega-i\gamma_{be})-\xi(\omega_{eg}/\omega_{be})(\omega_{eg}-\Omega-i\gamma_{eg})}{(\omega_{eg}-\Omega-i\gamma_{eg})^2(\omega_{eg}-\Omega+i\gamma_{eg})(\omega_{be}-\Omega-i\gamma_{be})}\gamma_{eg}^3$$
$$+2\xi\left[\frac{\Gamma_{eg}}{\gamma_{eg}}\right]\frac{2(\omega_{be}-\Omega-i\gamma_{be})-(\omega_{eg}/\omega_{be})(\omega_{eg}-\Omega-i\gamma_{eg})}{(\omega_{eg}-\Omega-i\gamma_{eg})^2(\omega_{bg}-2\Omega-i\gamma_{bg})(\omega_{be}-\Omega-i\gamma_{be})}\gamma_{eg}^3 . \quad (4.16)$$

From now on, we confine ourselves to the case where the transverse relaxation rates are much larger than the longitudinal relaxation rates, namely, the transverse relaxation rates are dominated by the pure dephasing rates. The dependence of $\chi^{(3)}$ on the exciton oscillator strength depends delicately on the character of the longitudinal relaxation rate Γ_{eg}. Two limiting cases for the longitudinal relaxation rate are considered: when the longitudinal relaxation is purely radiative and when it is dominated by the nonradiative decay. The first case is relevant to good quality samples. The longitudinal relaxation is given in terms of the oscillator strength as

$$\Gamma_{eg}=2\gamma'_{eg}=\frac{2ne^2\omega_{eg}^2}{3m_0c^3}F_{eg} , \quad (4.17)$$

where n is the refractive index of the material. In this case, $\chi^{(3)}$ is proportional to the oscillator strength and is given by

$$\chi^{(3)}=\frac{3e^2c^3}{4Lm_0n\hbar\omega_{eg}\Omega^3\gamma_{eg}^2}\left[\frac{2Q^2}{m_0\hbar\omega_{eg}}|p_{eg}|^2\right]h_0(\Omega) . \quad (4.18)$$

Thus the dependence of $\chi^{(3)}$ on material parameters is similar to that of the oscillator strength in (4.7). On the other hand, $\chi^{(3)}$ for the second case is proportional to the square of the oscillator strength, and thus depends more strongly on material parameters than the oscillator strength does. The absolute magnitude of $\chi^{(3)}$ and its dependence on material parameters will be discussed in the next section.

V. PRACTICAL EXAMPLES OF DQW's

In this section, some practical examples of DQW's are proposed. Here, we consider mainly a DQW with a GaAs well layer because its characteristics are well understood; for example, band gap, effective masses, dielectric constant, and band discontinuity to other materials. First, we will discuss the feasibility of fabricating DQW's. In fabricating heterointerfaces, one should first consider the lattice properties. In particular, the lattice structure and lattice constant are important quantities to be matched between the two materials to fabricate a high-quality interface. GaAs has a zincblende (cubic) structure and its lattice constant is 5.653 Å. From this point of view, materials are limited to such species as Ge, Al(Ga)As(P), Zn(S)Se, CaF_2, NaCl, or BaO. All these materials have cubic lattice structures and lattice constants similar to GaAs and larger band gaps than GaAs. Among them, Ge and BaO have larger static dielectric constants than GaAs and they are not appropriate for the barrier material of DQW's. Al(Ga)As(P) is one of the most popular materials to form heterointerfaces between GaAs. Many studies on the GaAs/ZnSe heterointerface have been reported.[15–17] However, the main concern of these studies was the epitaxial growth of ZnSe; GaAs is used only as a substrate with a similar lattice constant. Thus the DQW effect in this structure has not been noticed explicitly. Nevertheless, there is great possibility for fabricating the GaAs/ZnSe DQW's. Heteroepitaxial growth of CaF_2 has been studied.[18–20] However, since this material has a different lattice structure and a rather different thermal expansion coefficient from GaAs, a high-quality heterointerface is still very difficult to grow at present although high-quality growth of CaF_2 is expected in the near future. The situation for NaCl is similar to that for CaF_2. However, due to its deliquescent nature, a stable GaAs/NaCl heterointerface seems quite difficult to fabricate at present. Table V presents the material parameters of GaAs, $Al_{0.3}Ga_{0.7}As$, AlAs, ZnSe, CaF_2, and NaCl. Parameters for $Al_{0.3}Ga_{0.7}As$ are determined by linearly interpolating those of GaAs and AlAs.

Before going into detail, we will briefly discuss the dielectric constant to be used in the exciton problem. Mayer[21] and Haken[22] have proposed that the Coulomb interaction for the exciton has the following form:

$$V^{\text{Coulomb}}=-\frac{e^2}{\epsilon_\infty r}+\frac{e^2}{r}\left[\frac{1}{\epsilon_\infty}-\frac{1}{\epsilon_0}\right][1-\tfrac{1}{2}(e^{-q_e r}+e^{-q_h r})] \quad (5.1)$$

with $q_e=(2m_e\omega_{\text{LO}}/\hbar)^{1/2}$ and $q_h=(2m_h\omega_{\text{LO}}/\hbar)^{1/2}$, where r is the electron-hole distance, the static (optical) dielectric constant is denoted by ϵ_0 (ϵ_∞), and ω_{LO} represents the LO-phonon frequency. For GaAs, the LO-phonon energy $\hbar\omega_{\text{LO}}$ is about 35 meV, and the quantities q_e^{-1} and q_h^{-1} are 40 and 15 Å, respectively. For $r \gg 40$ Å the Coulomb interaction is determined by the static dielectric constant ϵ_0, while for $r \ll 15$ Å the Coulomb interaction is determined by the optical dielectric constant ϵ_∞. The excitonic Bohr radius in bulk GaAs is about 114 Å and thus the Coulomb interaction is dominantly determined by the static dielectric constant. However, in the DQW structure, especially in thin well layers, the excitonic Bohr radius becomes anisotropic and is reduced. Thus the situation becomes intermediate between the two limits, and an interpolation formula like (5.1) should be used. In the following, we will use the static dielectric constant ϵ_0, which yields the minimum value of the exciton binding energy, for GaAs/$Al_xGa_{1-x}As$, GaAs/AlAs, and GaAs/ZnSe DQW's. For GaAs/CaF_2 and GaAs/NaCl DQW's which have smaller exciton Bohr radius, both the static and the optical dielectric constants are used to show the minimum and maximum values of the exciton binding energy.

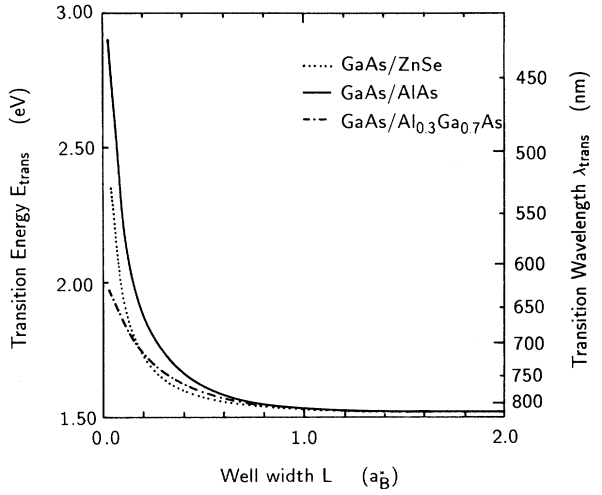

FIG. 14. Transition energy of the exciton for $GaAs/Al_{0.3}Ga_{0.7}As$, GaAs/AlAs, and GaAs/ZnSe DQW's. The energy gap of the bulk GaAs is taken to be 1.52 eV. The corresponding transition wavelength is also given in the figure.

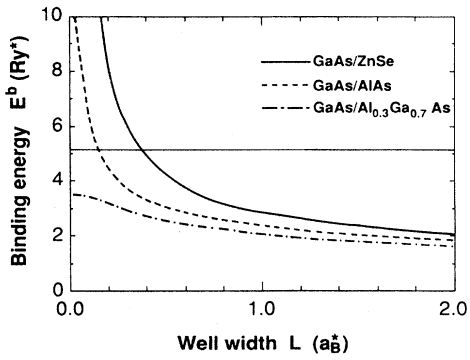

FIG. 15. Exciton binding energy for $GaAs/Al_{0.3}Ga_{0.7}As$, GaAs/AlAs, and GaAs/ZnSe DQW's. The material parameters used in the calculation are given in Table V.

Now let us consider the calculated results. First, the change in exciton transition energy will be discussed. Figure 14 gives the transition energy of the exciton in GaAs/ZnSe, GaAs/AlAs, and $GaAs/Al_{0.3}Ga_{0.7}As$ DQW's. The band-gap energy of bulk GaAs [E_g(GaAs)] is taken to be 1.52 eV, and the exciton transition energy is nearly the same as E_g(GaAs) for DQW's with well widths larger than $0.8a_B^*$. However, for thin well layers ($L \lesssim 0.4a_B^*$), the exciton transition energy increases drastically. These features are mainly determined by the well-width dependence of the subband energy because the exciton binding energy shows a much weaker dependence on the well thickness. In the limit of $L \to 0$, the exciton energy should approach that of the barrier material.

The calculated results of the exciton binding energy for $GaAs/Al_{0.3}Ga_{0.7}As$, GaAs/AlAs, and GaAs/ZnSe DQW's are shown as a function of the well width in Fig. 15. Throughout this section, the exciton binding energy and the well width are measured in units of the exciton binding energy of bulk GaAs ($\simeq 5$ meV), and exciton Bohr radius of bulk GaAs ($\simeq 114$ Å, respectively. The straight line in the figure gives the room-temperature energy ($k_B T \simeq 26$ meV). It can be seen that the GaAs/ZnSe

TABLE V. Parameters of the actual materials: GaAs, $Al_{0.3}Ga_{0.7}As$, AlAs, ZnSe, CaF_2, and NaCl. Notations are the same as in Table II. The static (optical) dielectric constant is denoted by ϵ_0 (ϵ_∞).

Materials	GaAs	$Al_{0.3}Ga_{0.7}As$[a]	AlAs	ZnSe	CaF_2	NaCl
lattice structure	zinc blende	zinc blende	zinc blende	zinc blende	CaF_2	NaCl
lattice constant (Å)	5.653	5.655	5.660	5.668	5.463	5.63
m_e (m_0)	0.0665[b]	0.084	0.124[c]	0.170[h]		
m_h (m_0)	0.475[c]	0.483	0.5[e]	0.57[i]		
ϵ_0	12.60[d]	11.84	10.06[f]	7.6[j]	6.8[l]	5.6[l]
ϵ_∞	10.9[d]	10.1	8.16[f]	5.4[j]	2[m]	2[m]
ΔE_c (eV)	0	0.32	1.06	0.34		
ΔE_v (eV)	0	0.17	0.55[g]	0.96[k]		

[a]These values are estimated by linear interpolation of the values of GaAs and AlAs.
[b]G. E. Stillman, D. M. Larsen, C. M. Wolfe, and R. C. Brandt, Solid State Commun. **9**, 2245 (1971).
[c]A. L. Mears and R. A. Stradling, J. Phys. C **4**, L22 (1971).
[d]C. J. Johnson, G. H. Sherman, and R. Weil, Appl. Opt. **8**, 1667 (1969).
[e]W. P. Dumke, M. R. Lorentz, and G. D. Pettit, Phys. Rev. B **5**, 2978 (1972).
[f]R. E. Fern and A. Onton, J. Appl. Phys. **42**, 3499 (1971).
[g]J. Batey and S. L. Wright, J. Appl. Phys. **59**, 200 (1986).
[h]D. T. F. Maple, J. Appl. Phys. **35**, 1879 (1964).
[i]M. Sondergeld, Phys. Status Solidi B **81**, 253 (1977).
[j]A. Manabe, A. Mitsuishi, and H. Yoshinaga, Jpn. J. Appl. Phys. **6**, 593 (1967).
[k]S. P. Kowalczyk, E. A. Kraut, J. R. Waldrop, and R. W. Grant, J. Vac. Sci. Technol. **21**, 482 (1982).
[l]*American Institute of Physics Handbook, 3rd ed.*, edited by D. E. Gray (McGraw-Hill, New York, 1982), pp. 9–74.
[m]*American Institute of Physics Handbook, 3rd ed.*, edited by D. E. Gray (McGraw-Hill, New York, 1982), pp. 6–12.

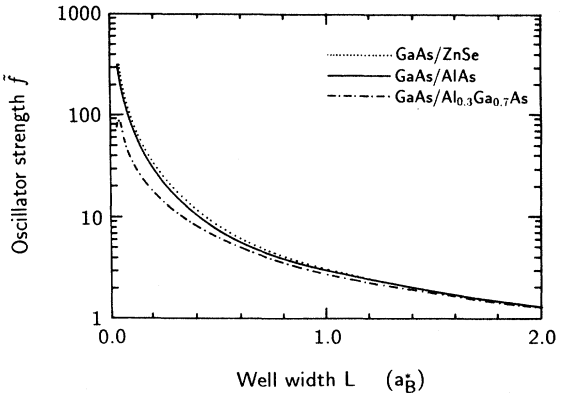

FIG. 16. Exciton oscillator strength of $GaAs/Al_{0.3}Ga_{0.7}As$, GaAs/AlAs, and GaAs/ZnSe DQW's normalized by the value of bulk GaAs.

DQW is favorable for getting a large exciton binding energy over the whole range of the well widths. $GaAs/Al_{0.3}Ga_{0.7}As$ DQW's have a smaller exciton binding energy than the others. These results agree well with the general features clarified in Sec. III because ZnSe has a smaller dielectric constant and larger carrier masses than GaAs, while $Al_{0.3}Ga_{0.7}As$ has similar values of the dielectric constant and carrier masses to GaAs.

Figure 16 shows the calculated oscillator strength of the excitonic transition for $Al_{0.3}Ga_{0.7}As/GaAs$, AlAs/GaAs, and ZnSe/GaAs DQW's. The general behavior of the oscillator strength is similar to that of the exciton binding energy, although the difference in the oscillator strength among three materials is smaller than that in the binding energy.

The absolute values of $\chi^{(3)}$ for $Al_{0.3}Ga_{0.7}As/GaAs$, AlAs/GaAs, and ZnSe/GaAs DQW's are shown in Fig. 17 as a function of the well width. In this calculation, the bulk value of the momentum matrix element p_{eg} and the transverse relaxation rate γ_{eg} are used as follows:

$$\frac{2p_{eg}^2}{m_0}=28.9 \text{ eV (Ref. 23)}, \tag{5.2}$$

$$\hbar\gamma_{eg}=2 \text{ meV (Ref. 4)}. \tag{5.3}$$

The spectral width Δ in (4.7) is assumed to be $2\hbar\gamma_{eg}$ and the dimensionless frequency factor $h_0(\Omega)$ in (4.16) is set to be unity. This calculation corresponds to the case where the longitudinal decay is purely radiative and thus the well-width dependence of $\chi^{(3)}$ is the same as that of the oscillator strength. The $GaAs/Al_{0.3}Ga_{0.7}As$ QW with a well width of 114 Å ($=a_B^*$) yields $\chi^{(3)}=0.06$ esu which agrees well with the experimental value.[4] Very large $\chi^{(3)}$ values can be achieved using a ZnSe barrier and reducing the well width.

Now the calculated results will be presented for GaAs DQW's with insulators as the barrier layer. The exciton binding energies of $GaAs/CaF_2$ and GaAs/NaCl DQW's are given in Fig. 18 as a function of the well width. The three curves correspond to three dielectric constants of the barrier medium of 2, 5.6, and 6.8 which are ϵ_∞ of both NaCl and CaF_2, ϵ_0 of NaCl, and ϵ_0 of CaF_2, respectively. The straight line in the figure gives the room-temperature energy. These curves were calculated using the infinite barrier model, because the band discontinuities between GaAs and these materials are unknown. Since these materials are both insulators and are considered to have very large band discontinuities with GaAs, the infinite barrier model is appropriate for these materials. Very large values of the exciton binding energy are obtained for both cases and the strong dependence on the dielectric constant of the barrier layer is demon-

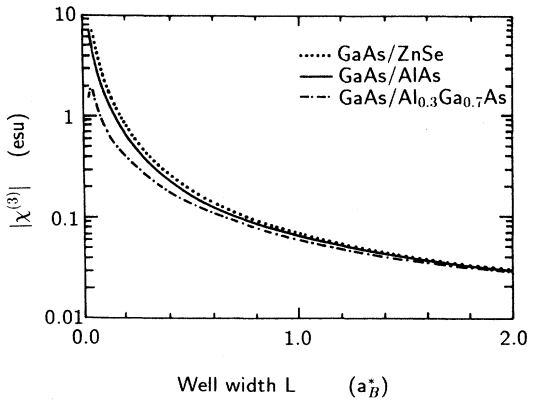

FIG. 17. Calculated third-order nonlinear susceptibility of $GaAs/Al_{0.3}Ga_{0.7}As$, GaAs/AlAs, and GaAs/ZnSe DQW's. These results are obtained by assuming that the longitudinal relaxation is dominated by the radiative decay which is directly related to the exciton oscillator strength.

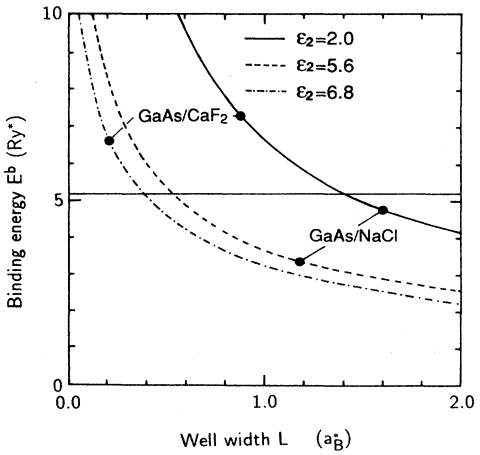

FIG. 18. Exciton binding energy of GaAs/NaCl and $GaAs/CaF_2$ DQW's. The static dielectric constants ϵ_0 of NaCl and CaF_2 are 5.6 and 6.8, respectively, and the optical dielectric constants ϵ_∞ of NaCl and CaF_2 are both 2.0. An infinite barrier model is used for the calculation, since the band discontinuities for these materials are not well known.

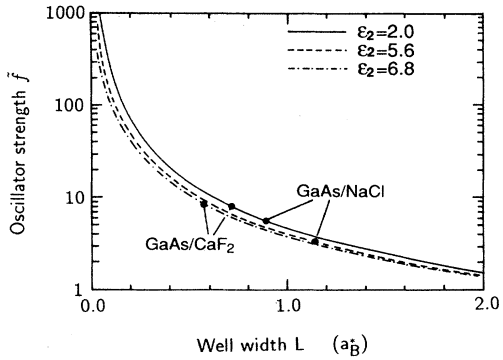

FIG. 19. Exciton oscillator strength of GaAs/NaCl and GaAs/CaF_2 DQW's normalized by the value of bulk GaAs. Material parameters used in the calculation are given in Table V.

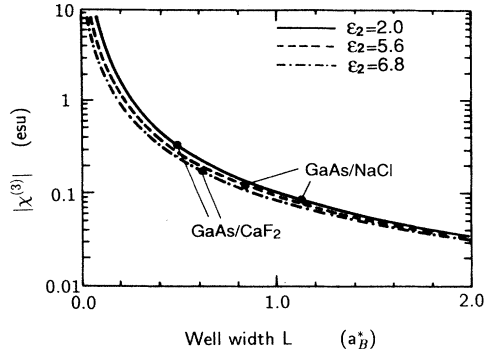

FIG. 20. Calculated third-order nonlinear susceptibility of GaAs/NaCl and GaAs/CaF_2 DQW's. The calculation used the same assumption as in Fig. 17.

strated. In this case, the absence of saturation of the exciton binding energy for very thin layers reflects the infiniteness of the barrier height. As mentioned above, the curves corresponding to ϵ_∞ and ϵ_0 give the maximum and minimum values of the exciton binding energy, respectively.

Figure 19 shows the oscillator strength of the excitonic transition in GaAs/CaF_2 and GaAs/NaCl DQW's. The well-width dependence is similar to that of the exciton binding energy; however, the dependence on dielectric constant is not so strong as that of the exciton binding energy. The absolute values of $\chi^{(3)}$ of these samples are given in Fig. 20 as a function of the well width. In these materials also, very large $\chi^{(3)}$ values can be expected.

Table VI summarizes the exciton binding energy, oscillator strength, radiative lifetime, and $\chi^{(3)}$ of GaAs DQW's with a well width $L=0.2a_B^*$ (=23 Å) for various barrier materials. DQW materials are clearly very promising for large exciton binding energy and large oscillator strength, and fast response time and large nonlinear susceptibility $\chi^{(3)}$.

Up to now, only DQW's with GaAs as the well material have been considered. However, there is no reason to restrict the well material to GaAs alone. Any material can be chosen as the well material for DQW's, and the key parameters are the energy of the excitonic transition, the exciton binding energy of the original material, and the feasibility of fabrication. For large exciton binding energy, a CuCl/CaF_2 DQW seems favorable as a practical example.[24] Also, DQW's with II-VI–compound semiconductors as the well material are favorable, because they originally have a large exciton binding energy in the bulk state.

Very recently, Ishihara *et al.* reported the excitonic properties of the two-dimensional perovskite semiconductor $(C_{10}H_{21}NH_3)_2PbI_4$.[25] This material consists of PbI_4 layers sandwiched between alkylammonium layers and has a typical DQW structure. They argued that the effective dielectric constant of PbI_4 layers is 13, while that of the organic layers is about 2. In their sample, the PbI_4 layer has a thickness of $0.3a_B^*$, where a_B^* is the exciton Bohr radius in bulk PbI_2 and the measured exciton binding energy is 12.3 Ry*. Since the band discontinuities and the effective masses of the alkylammonium are unknown, the infinite barrier model is employed in the calculation. Using the dielectric constant ratio ($\epsilon_1/\epsilon_2=6.5$) and the well thickness ($0.3a_B^*$), we estimate the exciton binding energy to be 15.5 Ry*, which agrees well with the experimental value. The enhancement factor of the oscillator strength relative to the bulk value is calculated to be 36, which agrees quite satisfactorily with the experimental value 41. They also observed the dependence of the exciton binding energy on the barrier thick-

TABLE VI. Calculated binding energy E^b, oscillator strength F_{eg}, radiative lifetime T_1, and third-order nonlinear optical susceptibility $\chi^{(3)}$ for the GaAs DQW's having 23-Å (=$0.2a_B^*$, where a_B^* is the exciton Bohr radius in bulk GaAs) -thick GaAs layer and barrier layers of $Al_{0.3}Ga_{0.7}As$, AlAs, ZnSe, CaF_2, and NaCl. The ϵ_0 or ϵ_∞ in parentheses is the dielectric constant of the barrier material employed in the calculation.

Barrier material	E^b (meV)	F_{eg}	T_1 (psec)	$\chi^{(3)}$ (esu)
$Al_{0.3}Ga_{0.7}As$ (ϵ_0)	15.7	40.3	211	0.42
AlAs (ϵ_0)	22.0	58.8	144	0.61
ZnSe (ϵ_0)	39.9	65.6	129	0.68
CaF_2 (ϵ_∞)	98.3	151	56.2	1.6
NaCl (ϵ_∞)	98.3	151	56.2	1.6

ness through the n dependence for $(C_nH_{2n+1}NH_3)_2PbI_4$ by varying the length of the alkylammonium chain.[26] They found an increase in the exciton binding energy with increasing n. This may be interpreted as the effect of the multiple quantum well (MQW). Although in our theory only a single-quantum-well (SQW) case is considered, the effect of the MQW can be simply deduced. In MQW structures, the carrier confinement effect, the carrier mass effect, and the dielectric confinement effect are all reduced because the wave functions and the electric force lines extend through several layers Thus, the exciton binding energy becomes larger with increasing n, approaching the value of the SQW case which corresponds to $n=\infty$.

VI. SUMMARY AND CONCLUSION

In this paper, the fundamental physics determining the excitonic properties in DQW's is clarified and, as a consequence, the guiding principles for designing DQW structures with optimum excitonic properties are obtained. (1) Exciton binding energy can be changed by varying the barrier height through the carrier confinement effect. In addition, the oscillator strength of excitonic transition and the nonlinear optical properties can be enhanced by enlarging the barrier height. (2) The carrier masses in barrier layers also affect the excitonic properties through the penetrating wave function. In general, the barrier material with heavier carrier masses yields a larger exciton binding energy, larger oscillator strength, and larger $\chi^{(3)}$. In this case, it is more effective to use barrier materials with heavy mass for the lighter carrier (electron) than for the heavier carrier (hole). (3) The dielectric constants of barrier layers affect the screening of the electron-hole Coulomb interaction and play an important role in determining the excitonic properties of the DQW. The excitonic properties are enhanced substantially by decreasing the barrier dielectric constant. Combining these general features, we can design the excitonic properties in DQW's to a great extent.

Some practical examples of DQW's have been proposed with GaAs as the well material. Here, ZnSe, which is a semiconducting barrier material, was shown to be one of the most favorable and promising materials. This is because it has a lattice constant nearly matched to GaAs, and has a smaller dielectric constant and larger carrier masses than GaAs. Furthermore, we can achieve a complete lattice matching by employing ZnS_xSe_{1-x} with a tiny amount of sulfur,[16] or $ZnSe/ZnS_xSe_{1-x}$ strained layer superlattice.[17]

Among the insulators, NaCl and CaF_2 are very favorable as barrier material of GaAs DQW's, because they have small dielectric constants and cubic lattice structures with a lattice constant nearly matched to GaAs.

This paper has considered the DQW structures exclusively. However, there is no reason to be limited to the DQW structure. Any structure with a heterointerface is expected to show enhanced excitonic properties. For example, even a single heterointerface can be expected to show the effect of dielectric confinement and effective-mass confinement. The quantum-well structure with different barrier materials on each side may also enhance excitonic properties. A thin single heterointerface can be considered as a DQW with a vacuum (air) layer as one of the barriers. Vacuum (air) is one of the best materials for the barrier of DQW's, because it has the smallest dielectric constant.

Furthermore, the DQW effect can be expected in other low-dimensional structures, namely quantum wires and quantum dot structures. Semiconductor microcrystallites are attracting much attention from both theoretical[27–31] and experimental[32–37] points of view. In zero-dimensional structures, the dielectric confinement and the quantum confinement effects are working in all space dimensions and thus the DQW effects appear significantly enhanced.[38]

Finally, we would like to mention other applications of the DQW structure. Generally speaking, the DQW structure changes not only the excitonic properties but also many other material properties, such as the mobility of the carrier ($\propto 1/m^*$), the CR time constant ($\propto \epsilon$), and the Fröhlich interaction $[(1/\epsilon_\infty - 1/\epsilon_0)^{1/2}]$. These properties play important roles in determining the performance of electronic devices as well as optical devices. Furthermore, the DQW structure is also effective for controlling the radiative lifetime, not only through the change of the oscillator strength mentioned in this paper, but through the change of the density of optical modes which depends on the electromagnetic dielectric constant of enlosing medium.[39]

In conclusion, the DQW structure is a unique material whose excitonic properties can be controlled to a great extent by changing the band discontinuity, carrier mass ratio, and the dielectric-constant ratio. This material whose has a large possibility to synthesize the novel properties which can be appropriate to our individual applications.

ACKNOWLEDGMENTS

The authors would like to thank Professor Eiichi Hanamura for stimulating discussions, Dr. Naoto Nagaosa for help in the formulation of the problem, and Dr. Takao Oono for his fruitful discussions. They also wish to thank Dr. Tatsuya Kimura for his interest in this work and his constant encouragement. Thanks are also due to Dr. Fumihiko Yanagawa and Dr. Yuuichi Kado for their helpful comments on the fabrication of the DQW.

APPENDIX A: COULOMB INTERACTIONS IN DIELECTRIC QUANTUM WELLS

This Appendix derives the Coulomb interaction between charged particles in dielectric quantum-well structures. The most general case will be considered in which the dielectric constants of the well layer (region I), the left-hand-side barrier layer (region II), and the right-hand-side barrier layer (region III) are given by ϵ_1, ϵ_2, and ϵ_3, respectively, as shown in Fig. 21(a). First of all, we calculate the electrostatic potential set up by a charged particle in the DQW structure. The discontinuity of the dielectric constant induces polarization charges at the interfaces. This polarization effect can be simply incor-

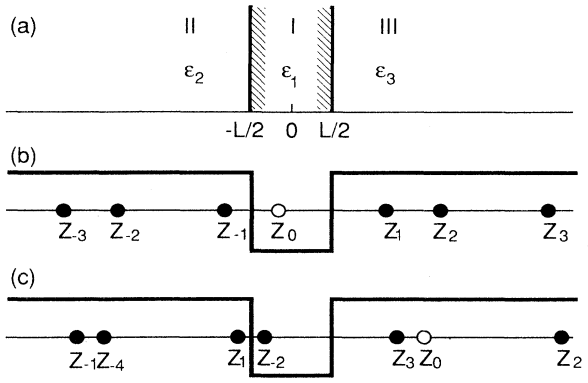

FIG. 21. (a) Schematic structure of a general three-layer DQW. Typical configurations of the real and image charges are shown for the cases when a charged particle is in the well layer (b), and in the right-hand-side barrier layer (c). The original charge is indicated by an open circle and the induced image charges are given by solid circles.

porated by the method of image charges.[40] However, in this case there is an infinite series of image charges due to the presence of two interfaces. The position of these image charges is given by

$$z_n = nL + (-1)^n z_0, \quad n = 0, \pm 1, \pm 2 \ldots , \tag{A1}$$

where z_0 denotes the position of the original charge, L is the thickness of the well layer, and the z axis is taken to be perpendicular to the interfaces. Three cases will be discussed separately depending on the position of the original charge.

Case I. The charged particle is in the well layer [region I in Fig. 21(a)]. A typical configuration of image charges is plotted in Fig. 21(b).

(a) The potential in region I is given by placing image charges $e_{\pm 1}$ and $e_{\pm 2}, \ldots$ at $z_{\pm 1}$ and $z_{\pm 2}, \ldots$, respectively, and at the same time by regarding the whole structure as having a common dielectric constant ϵ_1. The charges $\{e_n\}$ $(n = \pm 1, \pm 2, \ldots)$ are determined from the continuity conditions for the electrostatic potential and the normal component of the displacement vector at the interfaces. The results are given as

$$\begin{aligned} e_{\pm 2(n+1)} &= \xi^{n+1} e_0 , \\ e_{2n+1} &= \xi^n \frac{\epsilon_1 - \epsilon_3}{\epsilon_1 + \epsilon_3} e_0 , \\ e_{-2n-1} &= \xi^n \frac{\epsilon_1 - \epsilon_2}{\epsilon_1 + \epsilon_2} e_0 , \\ & \qquad n = 0, 1, 2, \ldots , \end{aligned} \tag{A2}$$

where e_0 is the original charge at z_0. The quantity ξ is defined by

$$\xi = \frac{\epsilon_1 - \epsilon_2}{\epsilon_1 + \epsilon_2} \frac{\epsilon_1 - \epsilon_3}{\epsilon_1 + \epsilon_3} . \tag{A3}$$

(b) The potential in region II (left-hand-side barrier layer) is given by placing image charges e'_0, e'_1, and $e'_2, \ldots$ at z_0, z_1, and $z_2, \ldots$ and at the same time by regarding the whole structure as having a common dielectric constant ϵ_2. The charges $\{e'_n\}$ $(n = 0, 1, 2, \ldots)$ are determined as

$$e'_n = \frac{2\epsilon_2}{\epsilon_1 + \epsilon_2} e_n, \quad n = 0, 1, 2, \ldots \tag{A4}$$

where the charges $\{e_n\}$ are given by (A2).

(c) The potential in region III (right-hand-side barrier layer) is given by placing image charges e''_0, e''_{-1}, and $e''_{-2}, \ldots$ at z_0, z_{-1}, and $z_{-2}, \ldots$ and by regarding the whole structure as having a common dielectric constant ϵ_3. The charges $\{e''_{-n}\}$ $(n = 0, 1, 2, \ldots)$ are given as

$$e''_{-n} = \frac{2\epsilon_3}{\epsilon_1 + \epsilon_3} e_{-n}, \quad n = 0, 1, 2, \ldots \tag{A5}$$

where the charges $\{e_{-n}\}$ are given by (A2).

Case II. The charged particle is in region II.

(a) The potential in region I is given by placing image charges e'_1, e'_3, and $e'_5, \ldots$ at z_1, z_3, and $z_5, \ldots$ and e'_0, e'_{-2}, and $e'_{-4}, \ldots$ at z_0, z_{-2}, and $z_{-4}, \ldots$, respectively, and by regarding the whole structure as having a common dielectric constant ϵ_1. The charges $\{e'_{2n+1}\}$ and $\{e'_{-2n}\}$ $(n = 0, 1, 2, \ldots)$ are determined as

$$e'_{2n+1} = \frac{2\epsilon_1}{\epsilon_1 + \epsilon_2} \frac{\epsilon_1 - \epsilon_3}{\epsilon_1 + \epsilon_3} \xi^n e_0, \quad e'_{-2n} = \frac{2\epsilon_1}{\epsilon_1 + \epsilon_2} \xi^n e_0 , \quad n = 0, 1, 2, \ldots . \tag{A6}$$

(b) The potential in region II is given by placing image charges e_{-1}, e_1, e_3, and $e_5, \ldots$ at z_{-1}, z_1, z_3, and $z_5, \ldots$ and by regarding the whole structure as having a common dielectric constant ϵ_2. The charges e_{-1} and $\{e_{2n+1}\}$ $(n = 0, 1, 2, \ldots)$ are given as

$$e_{-1} = -\frac{\epsilon_1 - \epsilon_2}{\epsilon_1 + \epsilon_2} e_0, \quad e_{2n+1} = \frac{4\epsilon_1 \epsilon_2}{(\epsilon_1 + \epsilon_2)^2} \frac{\epsilon_1 - \epsilon_3}{\epsilon_1 + \epsilon_3} \xi^n e_0 , \quad n = 0, 1, 2, \ldots . \tag{A7}$$

(c) The potential in region III is given by placing image charges e''_0, e''_{-2}, and $e''_{-4}, \ldots$ at z_0, z_{-2}, and $z_{-4}, \ldots$ and by regarding the whole structure as having a common dielectric constant ϵ_3. The charges $\{e''_{-2n}\}$ $(n = 0, 1, 2, \ldots)$ are given as

$$e''_{-2n} = \frac{4\epsilon_1 \epsilon_3}{(\epsilon_1 + \epsilon_2)(\epsilon_1 + \epsilon_3)} \xi^n e_0, \quad n = 0, 1, 2, \ldots . \tag{A8}$$

Case III. The charged particle is in region III. A typical configuration of image charges is plotted in Fig. 21(c).

(a) The potential in region I is given by placing image charges e'_0, e'_2, and $e'_4, \ldots$ at z_0, z_2, and $z_4, \ldots$ and e'_{-1}, e'_{-3}, and $e'_{-5}, \ldots$ at z_{-1}, z_{-3}, and $z_{-5}, \ldots$, respectively, and by regarding the whole structure as having a common dielectric constant ϵ_1. The charges $\{e'_{2n}\}$ and $\{e'_{-2n-1}\}$ $(n = 0, 1, 2, \ldots)$ are given as

$$e'_{2n}=\frac{2\epsilon_1}{\epsilon_1+\epsilon_3}\xi^n e_0,\quad e'_{-2n-1}=\frac{2\epsilon_1}{\epsilon_1+\epsilon_3}\frac{\epsilon_1-\epsilon_2}{\epsilon_1+\epsilon_2}\xi^n e_0\ ,$$
$$n=0,1,2,\ldots . \quad \text{(A9)}$$

(b) The potential in region II is given by placing image charges e''_0, e''_2, and e''_4,... at z_0, z_2, and z_4,... and by regarding the whole structure as having a common dielectric constant ϵ_2. The charges $\{e''_{2n}\}$ ($n=0,1,2,\ldots$) are given as

$$e''_{2n}=\frac{4\epsilon_1\epsilon_2}{(\epsilon_1+\epsilon_2)(\epsilon_1+\epsilon_3)}\xi^n e_0,\quad n=0,1,2,\ldots . \quad \text{(A10)}$$

(c) The potential in region III is given by placing image charges e_1, e_{-1}, e_{-3}, and e_{-5},... at z_1, z_{-1}, z_{-3}, and z_{-5},... and by regarding the whole structure as having a common dielectric constant ϵ_3. The charges e_1 and $\{e_{-2n-1}\}$ ($n=0,1,2,\ldots$) are given as

$$e_1=-\frac{\epsilon_1-\epsilon_3}{\epsilon_1+\epsilon_3}e_0,\quad e_{-2n-1}=\frac{4\epsilon_1\epsilon_3}{(\epsilon_1+\epsilon_3)^2}\frac{\epsilon_1-\epsilon_2}{\epsilon_1+\epsilon_2}\xi^n e_0\ ,$$
$$n=0,1,2,\ldots . \quad \text{(A11)}$$

Having obtained the electrostatic potential induced by a charged particle in the DQW structure, we can derive the Coulomb interaction between charged particles by calculating the potential at the position of a charged particle set up by another charged particle. For the electron-hole Coulomb interaction, we have six different interactions according to the position of an electron and a hole. Here, regions I, II, and III will be denoted by C, L, and R, respectively. Letting $H^{AB}_{\text{Coulomb}}(r_e,r_h)$ represent the Coulomb interaction between an electron in region A and a hole in region B, we have

$$H^{CC}_{\text{Coulomb}}(r_e,r_h)=-\sum_{n=-\infty}^{\infty}\frac{e^2\xi^{|n|}}{\epsilon_1[(r_{e\parallel}-r_{h\parallel})^2+(z_e-z_h-2nL)^2]^{1/2}}$$
$$-\frac{\epsilon_1-\epsilon_3}{\epsilon_1+\epsilon_3}\sum_{n=0}^{\infty}\frac{e^2\xi^n}{\epsilon_1\{(r_{e\parallel}-r_{h\parallel})^2+[z_e+z_h-(2n+1)L]^2\}^{1/2}}$$
$$-\frac{\epsilon_1-\epsilon_2}{\epsilon_1+\epsilon_2}\sum_{n=0}^{\infty}\frac{e^2\xi^n}{\epsilon_1\{(r_{e\parallel}-r_{h\parallel})^2+[z_e+z_h+(2n+1)L]^2\}^{1/2}}\ , \quad \text{(A12)}$$

$$H^{LL}_{\text{Coulomb}}(r_e,r_h)=-\frac{e^2}{\epsilon_2[(r_{e\parallel}-r_{h\parallel})^2+(z_e-z_h)^2]^{1/2}}$$
$$+\frac{\epsilon_1-\epsilon_2}{\epsilon_1+\epsilon_2}\frac{e^2}{\epsilon_2[(r_{e\parallel}-r_{h\parallel})^2+(z_e+z_h+L)^2]^{1/2}}$$
$$-\frac{4\epsilon_1\epsilon_2}{(\epsilon_1+\epsilon_2)^2}\frac{\epsilon_1-\epsilon_3}{\epsilon_1+\epsilon_3}\sum_{n=0}^{\infty}\frac{e^2\xi^n}{\epsilon_2\{(r_{e\parallel}-r_{h\parallel})^2+[z_e+z_h-(2n+1)L]^2\}^{1/2}}\ , \quad \text{(A13)}$$

$$H^{RR}_{\text{Coulomb}}(r_e,r_h)=-\frac{e^2}{\epsilon_3[(r_{e\parallel}-r_{h\parallel})^2+(z_e-z_h)^2]^{1/2}}$$
$$+\frac{\epsilon_1-\epsilon_3}{\epsilon_1+\epsilon_3}\frac{e^2}{\epsilon_3[(r_{e\parallel}-r_{h\parallel})^2+(z_e+z_h-L)^2]^{1/2}}$$
$$-\frac{4\epsilon_1\epsilon_3}{(\epsilon_1+\epsilon_3)^2}\frac{\epsilon_1-\epsilon_2}{\epsilon_1+\epsilon_2}\sum_{n=0}^{\infty}\frac{e^2\xi^n}{\epsilon_3\{(r_{e\parallel}-r_{h\parallel})^2+[z_e+z_h+(2n+1)L]^2\}^{1/2}}\ , \quad \text{(A14)}$$

$$H^{LC}_{\text{Coulomb}}(r_e,r_h)=-\frac{2}{\epsilon_1+\epsilon_2}\sum_{n=0}^{\infty}\frac{e^2\xi^n}{[(r_{e\parallel}-r_{h\parallel})^2+(z_e-z_h-2nL)^2]^{1/2}}$$
$$-\frac{2}{\epsilon_1+\epsilon_2}\frac{\epsilon_1-\epsilon_3}{\epsilon_1+\epsilon_3}\sum_{n=0}^{\infty}\frac{e^2\xi^n}{\{(r_{e\parallel}-r_{h\parallel})^2+[z_e+z_h-(2n+1)L]^2\}^{1/2}}\ , \quad \text{(A15)}$$

$$H^{LR}_{\text{Coulomb}}(r_e,r_h)=-\frac{4\epsilon_1}{(\epsilon_1+\epsilon_2)(\epsilon_1+\epsilon_3)}\sum_{n=0}^{\infty}\frac{e^2\xi^n}{[(r_{e\parallel}-r_{h\parallel})^2+(z_e-z_h-2nL)^2]^{1/2}}\ , \quad \text{(A16)}$$

$$H^{CR}_{\text{Coulomb}}(r_e,r_h)=-\frac{2}{\epsilon_1+\epsilon_3}\sum_{n=0}^{\infty}\frac{e^2\xi^n}{[(r_{e\parallel}-r_{h\parallel})^2+(z_e-z_h-2nL)^2]^{1/2}}$$
$$-\frac{2}{\epsilon_1+\epsilon_3}\frac{\epsilon_1-\epsilon_2}{\epsilon_1+\epsilon_2}\sum_{n=0}^{\infty}\frac{e^2\xi^n}{\{(r_{e\parallel}-r_{h\parallel})^2+[z_e+z_h+(2n+1)L]^2\}^{1/2}}\ . \quad \text{(A17)}$$

From the invariance of the Coulomb interaction under the exchange of sign of charges, we can show that

$H^{CL}_{\text{Coulomb}}(r_e,r_h)=H^{LC}_{\text{Coulomb}}(r_h,r_e)$, $H^{RL}_{\text{Coulomb}}(r_e,r_h)=H^{LR}_{\text{Coulomb}}(r_h,r_e)$, and $H^{RC}_{\text{Coulomb}}(r_e,r_h)=H^{CR}_{\text{Coulomb}}(r_h,r_e)$. Using these relations, we can obtain the electron-hole Coulomb interaction for all configurations of electron and hole positions.

Finally, for the sake of completeness, the self-energy due to the image charges will be given. The z coordinate of an electron or a hole will be denoted by z_0. Then we have the self-energy $H^{C}_{\text{self}}(r)$ of a charged particle in region I as

$$H^{C}_{\text{self}}(r)=\frac{e^2}{2\epsilon_1 L}\sum_{n=1}^{\infty}\frac{\xi^n}{n}+\frac{e^2}{2\epsilon_1}\frac{\epsilon_1-\epsilon_3}{\epsilon_1+\epsilon_3}\sum_{n=0}^{\infty}\frac{\xi^n}{|2z_0-(2n+1)L|}+\frac{e^2}{2\epsilon_1}\frac{\epsilon_1-\epsilon_2}{\epsilon_1+\epsilon_2}\sum_{n=0}^{\infty}\frac{\xi^n}{|2z_0+(2n+1)L|}\ . \tag{A18}$$

Similarly for charged particles in regions II and III, we obtain

$$H^{L}_{\text{self}}(r)=-\frac{e^2}{2\epsilon_2}\frac{\epsilon_1-\epsilon_2}{\epsilon_1+\epsilon_2}\frac{1}{|2z_0+L|}+\frac{2\epsilon_1 e^2}{(\epsilon_1+\epsilon_2)^2}\frac{\epsilon_1-\epsilon_3}{\epsilon_1+\epsilon_3}\sum_{n=0}^{\infty}\frac{\xi_n}{|2z_0-(2n+1)L|}\ , \tag{A19}$$

$$H^{R}_{\text{self}}(r)=-\frac{e^2}{2\epsilon_3}\frac{\epsilon_1-\epsilon_3}{\epsilon_1+\epsilon_3}\frac{1}{|2z_0-L|}+\frac{2\epsilon_1 e^2}{(\epsilon_1+\epsilon_3)^2}\frac{\epsilon_1-\epsilon_2}{\epsilon_1+\epsilon_2}\sum_{n=0}^{\infty}\frac{\xi^n}{|2z_0+(2n+1)L|}\ . \tag{A20}$$

For the case $\epsilon_2=\epsilon_3$, which is discussed in the text, the electron-hole Coulomb interaction and the self-energy are written as

$$H^{CC}_{\text{Coulomb}}(r_e,r_h)=-\sum_{n=-\infty}^{\infty}\frac{q_n e^2}{\epsilon_1\{(r_{e\parallel}-r_{h\parallel})^2+[z_e-(-1)^n z_h-nL]^2\}^{1/2}}\ , \tag{A21}$$

$$H^{LC}_{\text{Coulomb}}(r_e,r_h)=-\left[\frac{2\epsilon_1}{\epsilon_1+\epsilon_2}\right]\sum_{n=0}^{\infty}\frac{q_n e^2}{\epsilon_1\{(r_{e\parallel}-r_{h\parallel})^2+[z_e-(-1)^n z_h-nL]^2\}^{1/2}}\ , \tag{A22}$$

$$H^{RC}_{\text{Coulomb}}(r_e,r_h)=-\left[\frac{2\epsilon_1}{\epsilon_1+\epsilon_2}\right]\sum_{n=0}^{\infty}\frac{q_n e^2}{\epsilon_1\{(r_{e\parallel}-r_{h\parallel})^2+[z_e-(-1)^n z_h+nL]^2\}^{1/2}}\ , \tag{A23}$$

$$H^{LR}_{\text{Coulomb}}(r_e,r_h)=-\left[\frac{2\epsilon_1}{\epsilon_1+\epsilon_2}\right]^2\sum_{n=0}^{\infty}\frac{q_{2n}e^2}{\epsilon_1[(r_{e\parallel}-r_{h\parallel})^2+(z_e-z_h-2nL)^2]^{1/2}}\ , \tag{A24}$$

$$H^{RR}_{\text{Coulomb}}(r_e,r_h)=-\left[\frac{2\epsilon_1}{\epsilon_1+\epsilon_2}\right]^2\sum_{n=0}^{\infty}\frac{q_{2n+1}e^2}{\epsilon_1\{(r_{e\parallel}-r_{h\parallel})^2+[z_e+z_h+(2n+1)L]^2\}^{1/2}}$$
$$-\frac{e^2}{\epsilon_2[(r_{e\parallel}-r_{h\parallel})^2+(z_e-z_h)^2]^{1/2}}+\frac{q_1 e^2}{\epsilon_2[(r_{e\parallel}-r_{h\parallel})^2+(z_e+z_h-L)^2]^{1/2}}\ , \tag{A25}$$

$$H^{LL}_{\text{Coulomb}}(r_e,r_h)=H^{RR}_{\text{Coulomb}}(-r_e,-r_h)\ , \tag{A26}$$

$$H^{C}_{\text{self}}(r)=\frac{q_1 e^2}{2\epsilon_1|2z_0+L|}+\frac{q_1 e^2}{2\epsilon_1|2z_0-L|}+\sum_{n=\pm2,\pm3,\ldots}\frac{q_n e^2}{2\epsilon_1|z_0-(-1)^n z_0+nL|}\ , \tag{A27}$$

$$H^{R}_{\text{self}}(r)=-\frac{q_1 e^2}{2\epsilon_2|2z_0-L|}+\left[\frac{2\epsilon_1}{\epsilon_1+\epsilon_2}\right]\sum_{n=0}^{\infty}\frac{q_{2n+1}e^2}{(\epsilon_1+\epsilon_2)|2z_0+(2n+1)L|}\ , \tag{A28}$$

$$H^{L}_{\text{self}}(r)=H^{R}_{\text{self}}(-r)\ , \tag{A29}$$

where q_n is defined by

$$q_n=\left[\frac{\epsilon_1-\epsilon_2}{\epsilon_1+\epsilon_2}\right]^{|n|}\ , \tag{A30}$$

and is related to ξ in (A3) as

$$\xi|_{\epsilon_2=\epsilon_3}=q_2\ . \tag{A31}$$

The relations (A26) and (A29) are derived from the mirror symmetry with respect to the $z=0$ plane.

APPENDIX B: DISCUSSION ON THE BOUNDARY CONDITIONS FOR THE EFFECTIVE-MASS EQUATION

There are two methods of solving the one-particle state in the finite well. One is the conventional eigenvalue method which uses the stationary Schrödinger equation matching the energy eigenvalues in the well and the barrier regions. The other is the variational method which calculates the energy expectation value for the whole region and minimizes the value. These two methods yield different solutions in general, depending on the continuity

condition for the wave function and its first derivative. To see this situation more closely, the general derivation of the boundary condition is given below.

Here, we consider the case in which the whole space is divided into parts, and in each region the Hamiltonian is given by

$$H=-\frac{\hbar^2}{2m_i^*}\nabla^2+v(\mathbf{r}) , \tag{B1}$$

where m_i^* is the effective mass of the particle in region V_i. The corresponding Hamiltonian density h is given by a functional of the wave function ψ and its derivatives, i.e.,

$$h=h(\psi,\psi',\psi'',\psi^*,\psi^{*'},\psi^{*''})=-\frac{\hbar^2}{2m_i}\psi^*\nabla^2\psi+\psi^* v\psi \tag{B2}$$

for the region V_i, where the prime (double prime) means the first (second) derivative with respect to the spatial coordinates. Then the energy functional to be minimized is given by

$$E[\psi,\psi^*]=\frac{\int_V h(\psi,\psi',\psi'',\psi^*,\psi^{*'},\psi^{*''})d\mathbf{r}}{\int_V \psi^*\psi d\mathbf{r}} , \tag{B3}$$

where the region V consists of a number of subregions $\{V_i\}$.

We get the first variation as

$$\delta E\int_V\psi^*\psi\,d\mathbf{r}=\int_V(h_\psi\delta\psi+h_{\psi'}\delta\psi'+h_{\psi''}\delta\psi''-E\psi^*\delta\psi)d\mathbf{r}+\int_V(h_{\psi^*}\delta\psi^*+h_{\psi^{*'}}\delta\psi^{*'}+h_{\psi^{*''}}\delta\psi^{*''}-E\psi\delta\psi^*)d\mathbf{r} , \tag{B4}$$

where h_ξ is defined by

$$h_\xi\equiv\frac{\partial h}{\partial\xi} . \tag{B5}$$

Using the Gauss theorem, we can rewrite (B4) as

$$\begin{aligned}\delta E\int_V\psi^*\psi\,d\mathbf{r}=&\int_V[h_\psi-(\nabla h_{\psi'})+(\nabla^2 h_{\psi''})-E\psi^*]\delta\psi d\mathbf{r}+\int_S[h_{\psi'}\delta\psi+\nabla(h_{\psi''}\delta\psi)-2(\nabla h_{\psi''})\delta\psi]d\sigma\\&+\int_V[h_{\psi^*}-(\nabla h_{\psi^{*'}})+(\nabla^2 h_{\psi^{*''}})-E\psi^*]\delta\psi^* d\mathbf{r}+\int_S[h_{\psi^{*'}}\delta\psi^*+\nabla(h_{\psi^{*''}}\delta\psi^*)-2(\nabla h_{\psi^{*''}})\delta\psi^{star}]d\sigma .\end{aligned} \tag{B6}$$

Substituting the Hamiltonian density (B2) into (B6), we have

$$\begin{aligned}\delta E\int_V\psi^*\psi\,d\mathbf{r}=&\sum_i\int_{V_i}\left[-\frac{\hbar^2}{2m_i^*}\nabla^2+v-E\right]\psi\delta\psi^* d\mathbf{r}+\sum_i\int_{V_i}\left[-\frac{\hbar^2}{2m_i^*}\nabla^2+v-E\right]\psi^*\delta\psi d\mathbf{r}\\&+\sum_i\int_{S_i}\left[\nabla\left[-\frac{\hbar^2}{2m_i^*}\psi^*\delta\psi\right]-2\left[-\frac{\hbar^2}{2m_i^*}\nabla\psi^*\right]\delta\psi\right]d\sigma ,\end{aligned} \tag{B7}$$

where S_i denotes the surface of the region V_i. The eigenfunction of the Hamiltonian H is determined from the stationarity condition

$$\delta E=0 . \tag{B8}$$

Then, we obtain the Schrödinger equation

$$\left[-\frac{\hbar^2}{2m_i^*}\nabla^2+v-E\right]\psi=0 , \tag{B9}$$

with the following boundary condition:[41]

$$\sum_i\int_{S_i}\left[\nabla\left[-\frac{\hbar^2}{2m_i^*}\psi^*\delta\psi\right]-2\left[-\frac{\hbar^2}{2m_i^*}\nabla\psi^*\right]\delta\psi\right]d\sigma=0 . \tag{B10}$$

For the one-dimensional problem, this condition reduces to

$$\begin{aligned}-\sum_i\Bigg[&\left[-\frac{\hbar^2}{2m_i^*}\psi^*\frac{d}{dx}(\delta\psi)\right]_{x_{i,i+1}-0}-\left[-\frac{\hbar^2}{2m_{i+1}^*}\psi^*\frac{d}{dx}(\delta\psi)\right]_{x_{i,i+1}+0}\\&+\sum_i\left\{\left[-\frac{\hbar^2}{2m_i^*}\left[\frac{d\psi^*}{dx}\right]\delta\psi\right]_{x_{i,i+1}-0}-\left[-\frac{\hbar^2}{2m_{i+1}^*}\left[\frac{d\psi^*}{dx}\right]\delta\psi\right]_{x_{i,i+1}+0}\right\}=0 ,\end{aligned} \tag{B11}$$

where $x_{i,i+1}$ stands for the coordinate of the interface between the ith and $(i+1)$th regions, and the suffix $+0$ (-0) indicates the right- (left-) hand side of the interface. If we suppose the independence of $\delta\psi$ at the interfaces, we can drop

the summation over the suffix i in (B11) and obtain

$$-\left[\left[-\frac{\hbar^2}{2m_i^*}\psi^*\frac{d}{dx}(\delta\psi)\right]_{x_{i,i+1}-0}-\left[-\frac{\hbar^2}{2m_{i+1}^*}\psi^*\frac{d}{dx}(\delta\psi)\right]_{x_{i,i+1}+0}\right]$$
$$+\left\{\left[-\frac{\hbar^2}{2m_i^*}\left[\frac{d\psi^*}{dx}\right]\delta\psi\right]_{x_{i,i+1}-0}-\left[-\frac{\hbar^2}{2m_{i+1}^*}\left[\frac{d\psi^*}{dx}\right]\delta\psi\right]_{x_{i,i+1}+0}\right\}=0\ . \quad \text{(B12)}$$

These conditions for the effective-mass wave function are quite general and are applicable to the case in which the effective-mass wave function is not continuous at the interfaces.[42] If we assume the continuity of the wave function as

$$\psi|_{x_{i,i+1}-0}=\psi|_{x_{i,i+1}+0}\ , \quad \text{(B13)}$$

the boundary condition (B12) is consistently satisfied by imposing

$$\frac{1}{m_i^*}\frac{d\psi}{dx}\bigg|_{x_{i,i+1}-0}=\frac{1}{m_{i+1}^*}\frac{d\psi}{dx}\bigg|_{x_{i,i+1}+0}\ . \quad \text{(B14)}$$

This continuity condition has the same form as that derived by Bastard,[43] and is employed in the text.

When we employ the continuity condition (B13) and a boundary condition

$$\frac{d\psi}{dx}\bigg|_{x_{i,i+1}-0}=\frac{d\psi}{dx}\bigg|_{x_{i,i+1}+0}\ , \quad \text{(B15)}$$

we find different solutions from the variational method and from the eigenvalue method of the Schrödinger equation. This discrepancy arises from the failure to satisfy the minimal constraint (B14) associated with the continuity condition (B13). In fact, when we adopt (B13) and (B14) consistently, we obtain exactly the same solutions from both approaches.

For a more general form of the boundary condition[42] given by

$$\begin{bmatrix}\psi\\ \psi'\end{bmatrix}\bigg|_{x_{i,i+1}+0}=\begin{bmatrix}a & b\\ c & d\end{bmatrix}\begin{bmatrix}\psi\\ \psi'\end{bmatrix}\bigg|_{x_{i,i+1}-0}\ , \quad \text{(B16)}$$

the boundary condition (B12) yields a constraint, i.e.,

$$1-\frac{m_i}{m_{i+1}}(ad-bc)=0\ . \quad \text{(B17)}$$

However, the condition (B12) cannot determine a, b, c, or d any further without going into details of the material structures. Thus the condition (B12) provides a minimal constraint which any model of the boundary condition for the effective-mass wave function must satisfy.

APPENDIX C: CALCULATION OF THE EXPECTATION VALUE OF THE HAMILTONIAN

Here, details of the calculation of various energy terms in Sec. II are presented. The expectation value of an operator X for the excitonic state in (2.21) is defined by

$$\langle\langle X\rangle\rangle=\int\int\int[A\psi_e(z_e)\psi_h(z_h)g(\mathbf{r}_\parallel,z_e-z_h)]\cdot X\cdot[A\psi_e(z_e)\psi_h(z_h)g(\mathbf{r}_\parallel,z_e-z_h)]d\mathbf{r}_\parallel dz_e dz_h\ , \quad \text{(C1)}$$

where the integration is taken over the whole region. The Fourier transform of the function g^2 is introduced to reduce the dimension of numerical integration:

$$g^2(\mathbf{r}_\parallel,z_e,z_h)=\exp\{-2[\alpha^2 r_\parallel^2+\beta^2(z_e-z_h)^2]^{1/2}\}=\int\frac{1}{\pi^2(k^2+1)}e^{i2\alpha\mathbf{k}_\parallel\cdot\mathbf{r}_\parallel+i2\beta k_z(z_e-z_h)}d\mathbf{k}\ . \quad \text{(C2)}$$

(1) *Calculation of the normalization constant A.* The normalization constant A is necessary to calculate the expectation value (C1) and is determined by the following equation:

$$1=\int\int\int\int A^2\psi_e(z_e)^2\psi_h(z_h)^2\frac{1}{\pi^2(k^2+1)^2}e^{i2\alpha\mathbf{k}_\parallel\cdot\mathbf{r}_\parallel+i2\beta k_z(z_e-z_h)}d\mathbf{k}d\mathbf{r}_\parallel dz_e dz_h\ . \quad \text{(C3)}$$

Using the relations

$$\int e^{i(2\alpha\mathbf{k}_\parallel\cdot\mathbf{r}_\parallel)}d\mathbf{r}_\parallel=(2\pi)^2\delta(2\alpha\mathbf{k}_\parallel)=\left[\frac{\pi}{\alpha}\right]^2\delta(\mathbf{k}_\parallel) \quad \text{(C4)}$$

and

$$\int_{-\infty}^{+\infty}\frac{1}{\pi^2(k_z^2+1)^2}e^{i2\beta k_z(z_e-z_h)}dk_z=\frac{1}{\pi}[e^{-2\beta|z_e-z_h|}(\beta|z_e-z_h|+\tfrac{1}{2})]\ , \quad \text{(C5)}$$

we can reduce (C3) to

$$1=(4\pi^3)\int_{-\infty}^{+\infty}\int_{-\infty}^{+\infty}A^2\psi_e^2(z_e)\psi_h^2(z_h)(\beta|z_e-z_h|+\tfrac{1}{2})e^{-2\beta|z_e-z_h|}dz_e dz_h \ . \tag{C6}$$

In the integrand, ψ is a simple exponential function or a cosine function, and the integration can be carried out analytically.

(2) *Calculation of the kinetic-energy term.* The kinetic energy can be written as

$$\begin{aligned}E_{\rm kin}&=E_{\rm kin}^{(e)}+E_{\rm kin}^{(h)}\\&=-\sum_j\frac{\hbar^2}{2m_e^{(j)}}\int\int\int\int_{V_j}\Psi\nabla_e^2\Psi r_\parallel dr_\parallel d\theta\, dz_e dz_h-\sum_j\frac{\hbar^2}{2m_h^{(j)}}\int\int\int\int_{V_j}\Psi\nabla_h^2\Psi r_\parallel dr_\parallel d\theta\, dz_e dz_h \ ,\end{aligned} \tag{C7}$$

where the suffix j specifies the region V_j in which the effective mass is constant. Using the identity for a scalar field ϕ and a vector field $\mathbf{A}$,

$$\nabla\cdot(\phi\,\mathbf{A})=\phi(\nabla\cdot\mathbf{A})+\mathbf{A}\cdot(\nabla\phi) \ , \tag{C8}$$

the first term of (C7) can be rewritten as

$$E_{\rm kin}^{(e)}=-\sum_j\frac{\hbar^2}{2m_e^{(j)}}\int\int_{V_j}\nabla_e(\Psi\nabla_e\Psi)dV_e dz_h+\sum_j\frac{\hbar^2}{2m_e^{(j)}}\int\int_{V_j}(\nabla_e\Psi)^2dV_e dz_h \ , \tag{C9}$$

where the volume element is defined by $dV_e=r_\parallel dr_\parallel d\theta dz_e$. Applying the Gauss theorem to the first term, we have

$$E_{\rm kin}^{(e)}=-\sum_j\frac{\hbar^2}{2m_e^{(j)}}\int\int_{\sigma_j}\Psi\nabla_e\Psi dS_e dz_h+\sum_j\frac{\hbar^2}{2m_e^{(j)}}\int\int_{V_j}(\nabla_e\Psi)^2dV_e dz_h \ , \tag{C10}$$

where σ_j is the surface of the region V_j and dS_e denotes the surface element. Substitution of the expression of Ψ in (2.21) into (C10) leads to

$$\begin{aligned}E_{\rm kin}^{(e)}&=-\sum_j\frac{A^2\hbar^2}{2m_e^{(j)}}\int\int_{\sigma_j}(\psi_e\nabla_e\psi_e\psi_h^2g^2+\psi_e^2\psi_h^2g\nabla_e g)dS_e dz_h\\&\quad+\sum_j\frac{A^2\hbar^2}{2m_e^{(j)}}\int\int_{V_j}[\psi_h^2(\nabla_e\psi_e)^2g^2-\psi_e^2\psi_h^2g\nabla_e^2g+\nabla_e(\psi_e^2\psi_h^2g\nabla_e g)]dV_e dz_h\\&=-\sum_j\frac{A^2\hbar^2}{2m_e^{(j)}}\int\int_{\sigma_j}\psi_e\nabla_e\psi_e\psi_h^2g^2dS_e dz_h\\&\quad+\sum_j\frac{A^2\hbar^2}{2m_e^{(j)}}\int\int_{V_j}[\psi_h^2(\nabla_e\psi_e)^2g^2-\psi_e^2\psi_h^2g\nabla_e^2g]dV_e dz_h \ .\end{aligned} \tag{C11}$$

Clearly the first integral in (C11) vanishes due to the boundary conditions (2.17) and (2.18). Thus, we have

$$E_{\rm kin}^{(e)}=\sum_j\frac{A^2\hbar^2}{2m_e^{(j)}}\left[\int\int\psi_h^2(\nabla_e\psi_e)^2g^2dV_e dz_h-\int\int\psi_e^2\psi_h^2g\nabla_e^2g\,dV_e dz_h\right] . \tag{C12}$$

The second term of this expression can be reduced in a similar way to that used in (1). Finally, the electron kinetic energy can be expressed as follows:

$$\begin{aligned}E_{\rm kin}^{(e)}&=\sum_j\frac{A^2\hbar^2}{2m_e^{(j)}}\int\int\int\psi_h^2(\nabla_e\psi_e)^2g^2d\mathbf{r}_\parallel dz_e dz_h\\&\quad-\sum_j\frac{2\pi}{\alpha^2}\frac{A^2\hbar^2}{2m_e^{(j)}}\int\int\int\psi_e^2\psi_h^2e^{-2\beta(k_\parallel^2+1)^{1/2}|z_e-z_h|}\frac{\beta|z_e-z_h|+1/(k_\parallel^2+1)^{1/2}}{k_\parallel^2+1}\\&\qquad\times\left[\frac{(\alpha^2-\beta^2)k_\parallel^2-\beta^2}{k_\parallel^2+1}\beta|z_e-z_h|+\frac{(\alpha^2+\beta^2)k_\parallel^2+\beta^2}{(k_\parallel^2+1)^{3/2}}\right]k_\parallel dz_e dz_h dk_\parallel \ .\end{aligned} \tag{C13}$$

The first term can be calculated analytically. The second term can be integrated over z_e and z_h analytically, and the remaining integral over $k_\parallel$ is achieved numerically. The hole kinetic energy, namely the second term of (C7) can be calculated in exactly the same way.

(3) *Calculation of the Coulomb interaction term.* The Coulomb interaction energy can be expressed as

$$E_{\rm Coulomb}=\int\int\int A^2\psi_e^2\psi_h^2g^2H_{\rm Coulomb}d\mathbf{r}_\parallel dz_e dz_h \ . \tag{C14}$$

To reduce this expression to a more tractable form, it is useful to introduce the Fourier transform of g^2 in (C2) and

H_{Coulomb}. Here, the Fourier transform of H_{Coulomb} for the *CC* case (both electron and hole are in the well) will be derived. The results for other cases can be obtained similarly.

The Coulomb interaction Hamiltonian H_{Coulomb} for the *CC* case is given by (2.8), and can be expressed as

$$\begin{aligned} H_{\text{Coulomb}}(CC) = &- \sum_{n=0}^{\infty} \frac{e^2 q_{2n}}{\epsilon_1[(r_{e\parallel}-r_{h\parallel})^2+(z_e-z_h-2nL)^2]^{1/2}} \\ &- \sum_{n=0}^{\infty} \frac{e^2 q_{2n+1}}{\epsilon_1\{(r_{e\parallel}-r_{h\parallel})^2+[z_e+z_h-(2n+1)L]^2\}^{1/2}} \\ &- \sum_{n=0}^{\infty} \frac{e^2 q_{2n+2}}{\epsilon_1\{(r_{e\parallel}-r_{h\parallel})^2+[z_e-z_h+2(n+1)L]^2\}^{1/2}} \\ &- \sum_{n=0}^{\infty} \frac{e^2 q_{2n+1}}{\epsilon_1\{(r_{e\parallel}-r_{h\parallel})^2+[z_e+z_h+(2n+1)L]^2\}^{1/2}} . \end{aligned} \tag{C15}$$

Using the relation

$$\begin{aligned} \frac{1}{r} &= \frac{1}{2\pi^2}\int \frac{e^{i\mathbf{k}\cdot\mathbf{r}}}{k^2} d\mathbf{k} \\ &= \frac{1}{2\pi^2}\int \left[\int \frac{e^{ik_z z}}{k_\parallel^2+k_z^2} dk_z\right] e^{i\mathbf{k}_\parallel\cdot\mathbf{r}_\parallel} d\mathbf{k}_\parallel \\ &= \frac{1}{2\pi}\int \frac{1}{k_\parallel} e^{-|\mathbf{k}_\parallel||z|+i\mathbf{k}_\parallel\cdot\mathbf{r}_\parallel} d\mathbf{k}_\parallel , \end{aligned} \tag{C16}$$

(C15) can be rewritten as

$$\begin{aligned} H^{CC}_{\text{Coulomb}} = -\frac{e^2}{2\pi\epsilon_1}\sum_{n=0}^{\infty}\int \frac{1}{k} e^{i\mathbf{k}_\parallel\cdot\mathbf{r}_\parallel}(&e^{-(z_>-z_<)k} e^{-2n(kL+\eta)} + e^{(z_>+z_<)k} e^{-(2n+1)(kL+\eta)} \\ &+ e^{(z_>-z_<)k} e^{-2(n+1)(kL+\eta)} + e^{-(z_>+z_<)k} e^{-2(n+1)(kL+\eta)}) d\mathbf{k}_\parallel , \end{aligned} \tag{C17}$$

where $k=|k_\parallel|$, $\mathbf{r}_\parallel=\mathbf{r}_{e\parallel}-\mathbf{r}_{h\parallel}$, $z_>=\max(z_e,z_h)$, $z_<=\min(z_e,z_h)$, and η is defined by

$$q_n = \left[\frac{\epsilon_1-\epsilon_2}{\epsilon_1+\epsilon_2}\right]^{|n|} \equiv (e^{-\eta})^{|n|} . \tag{C18}$$

Summing up the four geometric series, we have

$$H^{CC}_{\text{Coulomb}} = -\frac{e^2}{\pi\epsilon_1}\int e^{i\mathbf{k}_\parallel\cdot\mathbf{r}_\parallel}\frac{\cosh[(z_<+L/2)k+\eta/2]\cosh[(z_>-L/2)k-\eta/2]}{k\sinh(kL+\eta)} d\mathbf{k}_\parallel . \tag{C19}$$

The integration in (C14) over $\mathbf{r}_\parallel$, z_e, and z_h can be achieved analytically in the same way as in (1) and (2). The remaining integral over k is achieved numerically. Finally, for the sake of completeness, the Fourier transforms of the Coulomb interaction for other cases are given as follows:

$$H^{LC}_{\text{Coulomb}} = -\frac{e^2}{\pi(\epsilon_1+\epsilon_2)}\int e^{i\mathbf{k}_\parallel\cdot\mathbf{r}_\parallel} e^{(L/2+z_e)k+\eta/2}\frac{\cosh[(L/2+z_h)k+\eta/2]}{k\sinh(kL+\eta)} d\mathbf{k}_\parallel , \tag{C20}$$

$$H^{RC}_{\text{Coulomb}} = -\frac{e^2}{\pi(\epsilon_1+\epsilon_2)}\int e^{i\mathbf{k}_\parallel\cdot\mathbf{r}_\parallel} e^{(L/2-z_e)k+\eta/2}\frac{\cosh[(L/2-z_h)k+\eta/2]}{k\sinh(kL+\eta)} d\mathbf{k}_\parallel , \tag{C21}$$

$$H^{LR}_{\text{Coulomb}} = -\frac{e^2\epsilon_1}{\pi(\epsilon_1+\epsilon_2)^2}\int e^{i\mathbf{k}_\parallel\cdot\mathbf{r}_\parallel}\frac{e^{[(L/2+z_e)k+\eta/2]} e^{[(L/2-z_h)k+\eta/2]}}{k\sinh(kL+\eta)} d\mathbf{k}_\parallel , \tag{C22}$$

$$\begin{aligned} H^{RR}_{\text{Coulomb}} = &-\frac{e^2}{2\pi\epsilon_2}\int e^{i\mathbf{k}_\parallel\cdot\mathbf{r}_\parallel}\frac{e^{-|z_e-z_h|k}}{k} d\mathbf{k}_\parallel + \frac{e^2}{2\pi\epsilon_2}\left[\frac{\epsilon_1-\epsilon_2}{\epsilon_1+\epsilon_2}\right]\int e^{i\mathbf{k}_\parallel\cdot\mathbf{r}_\parallel}\frac{e^{-(z_e+z_h-L)k}}{k} d\mathbf{k}_\parallel \\ &-\frac{e^2\epsilon_1}{\pi(\epsilon_1+\epsilon_2)^2}\int e^{i\mathbf{k}_\parallel\cdot\mathbf{r}_\parallel}\frac{e^{-(z_e+z_h)k}}{k\sinh(kL+\eta)} d\mathbf{k}_\parallel . \end{aligned} \tag{C23}$$

[1]*Semiconductors and Semimetals*, edited by R. Dingle (Academic, New York, 1987), Vol. 24.
[2]D. A. B. Miller, D. S. Chemla, T. C. Damen, A. C. Gossard, W. Wiegmann, T. H. Wood, and C. A. Burrus, Appl. Phys. Lett. **45**, 13 (1984).
[3]D. A. B. Miller, D. S. Chemla, T. C. Damen, A. C. Gossard, W. Wiegmann, T. H. Wood, and C. A. Burrus, Phys. Rev. B **32**, 1043 (1985).
[4]D. S. Chemla, D. A. B. Miller, P. W. Smith, A. C. Gossard, and W. Wiegman, IEEE J. Quantum Electron. **QE-20**, 265 (1984).
[5]M. Shinada and S. Sugano, J. Phys. Soc. Jpn. **21**, 1936 (1966).
[6]L. V. Keldysh, Pis'ma Zh. Eksp. Teor. Fiz. **29**, 716 (1979) [JETP Lett. **29**, 658 (1979)].
[7]L. V. Keldysh, Superlatt. Microstruct. **4**, 637 (1966).
[8]E. Hanamura, N. Nagaosa, M. Kumagai, and T. Takagahara, Mater. Sci. Eng. B **1**, 255 (1988).
[9]M. Kumagai and T. Takagahara, *Extended Abstracts of the 20th International Conference on Solid State Devices and Materials* (The Japan Society of Applied Physics, Tokyo, 1988), p. 335.
[10]N. D. Lang and W. Kohn, Phys. Rev. B **7**, 3541 (1973)
[11]R. S. Knox, *Theory of Excitons* (Academic, New York, 1963), Suppl. 5.
[12]Y. R. Shen, *The Principles of Nonlinear Optics* (Wiley-Interscience, New York, 1984).
[13]T. Takagahara, Phys. Rev. B **39**, 10 206 (1989); T. Takagahara and M. Kumagai (unpublished).
[14]J. Feldmann, G. Peter, E. O. Göbel, P. Dawson, K. Moore, C. Foxon, and R. J. Elliott, Phys. Rev. Lett. **59**, 2337 (1987).
[15]W. Studius, J. Electron. Mater. **10**, 95 (1981).
[16]N. Matsumura, M. Tsubokura, K. Ishikawa, J. Saraie, and Y. Yodogawa, J. Cryst. Growth **86**, 311 (1988).
[17]S. Fujita, Y. Matsuda, and A. Sasaki, Appl. Phys. Lett. **47**, 955 (1985).
[18]L. J. Schowalter and R. W. Fathauer, J. Vac. Sci. Technol. A **4**, 1026 (1986).
[19]K. Tsutsui, H. Ishiwara, and S. Furukawa, Appl. Phys. Lett. **48**, 587 (1986).
[20]S. Siskos, C. Fontaine, and A. Munoz-Yague, Appl. Phys. Lett. **44**, 1146 (1984).
[21]H. J. G. Mayer, Physica **22**, 109 (1956).
[22]H. Haken, J. Phys. Chem. Solids **8**, 166 (1959).
[23]C. Weisbuch and R. G. Ulbrich, in *Light Scattering in Solids III*, edited by M. Cardona and G. Güntherodt (Springer, Berlin, 1982), Chap. 7.
[24]R. S. Williams, D. K. Shur, and Y. Segawa, J. Vac. Sci. Technol. A **6**, 1950 (1988).
[25]T. Ishihara, J. Takahashi, and T. Goto, Solid State Commun. **69**, 933 (1989).
[26]T. Ishihara (private communication).
[27]Al. L. Efros and A. L. Efros, Fiz. Tekh. Poluprovodn. **16**, 1209 (1982) [Sov. Phys.—Semicond. **16**, 772 (1982)].
[28]L. E. Brus, IEEE J. Quantum Electron. **QE-22**, 1909 (1986), and references therein.
[29]Y. Kayanuma, Solid State Commun. **59**, 405 (1986).
[30]T. Takagahara, Phys. Rev. B **36**, 9293 (1987).
[31]E. Hanamura, Phys. Rev. B **37**, 1273 (1988).
[32]R. K. Jain and R. C. Lind, J. Opt. Soc. Am. **73**, 647 (1983).
[33]G. R. Olbright and N. Peyghambarian, Appl. Phys. Lett. **48**, 1184 (1986).
[34]J. Yumoto, S. Fukushima, and K. Kubodera, Opt. Lett. **12**, 832 (1987).
[35]T. Itoh, Y. Iwabuchi, and M. Kataoka, Phys. Status Solidi B **145**, 567 (1988).
[36]T. Itoh, Y. Iwabuchi, and T. Kirihara, Phys. Status Solidi B **146**, 531 (1988).
[37]M. Mitsunaga, H. Shinojima, and K. Kubodera, J. Opt. Soc. Am. B **5**, 1448 (1988).
[38]T. Takagahara, *Technical Digest of the XVIth International Conference on Quantum Electronics* (The Japan Society of Applied Physics, Tokyo, 1980), p. 620.
[39]E. Yablonovitch, T. J. Gmitter, and R. Bhat, Phys. Rev. Lett. **61**, 2546 (1988).
[40]W. K. H. Panofsky and M. Phillips, *Classical Electricity and Magnetism* (Addison-Wesley, Cambridge, 1961).
[41]P. M. Morse and H. Feshbach, *Methods of Theoretical Physics* (McGraw-Hill, New York, 1953).
[42]T. Ando and S. Mori, Surf. Sci. **113**, 124 (1982).
[43]G. Bastard, Phys. Rev. B **24**, 5693 (1981).